CELL BIOLOGY

Soft extracellular matrix enhances inflammatory activation of mesenchymal stromal cells to induce monocyte production and trafficking

Sing Wan Wong[1], Stephen Lenzini[1], Madeline H. Cooper[2]*, David J. Mooney[2†], Jae-Won Shin[1†]

Mesenchymal stromal cells (MSCs) modulate immune cells to ameliorate multiple inflammatory pathologies. Biophysical signals that regulate this process are poorly defined. By engineering hydrogels with tunable biophysical parameters relevant to bone marrow where MSCs naturally reside, we show that soft extracellular matrix maximizes the ability of MSCs to produce paracrine factors that have been implicated in monocyte production and chemotaxis upon inflammatory stimulation by tumor necrosis factor–α (TNFα). Soft matrix increases clustering of TNF receptors, thereby enhancing NF-κB activation and downstream gene expression. Actin polymerization and lipid rafts, but not myosin-II contractility, regulate mechanosensitive activation of MSCs by TNFα. We functionally demonstrate that human MSCs primed with TNFα in soft matrix enhance production of human monocytes in marrow of xenografted mice and increase trafficking of monocytes via CCL2. The results suggest the importance of biophysical signaling in tuning inflammatory activation of stromal cells to control the innate immune system.

INTRODUCTION

Mesenchymal stromal cells (MSCs) in bone marrow (BM) consist of different subpopulations with multiple biological functions, including multipotent differentiation (*1*), maintenance of hematopoietic stem cells (HSCs) (*2*), and immunomodulation (*3*). The role of MSCs in immunomodulation has been shown mostly in the context of adoptive transfer where plastic-adherent cells derived from the BM are expanded in vitro and administered to treat diverse inflammatory pathologies (*4*). Thus, it remains generally unclear how physiologically relevant signals from the extracellular matrix (ECM) in the BM microenvironment regulate these immunomodulatory functions of MSCs. Since MSCs show preclinical efficacy in some disease models without long-term engraftment (*5*), it has been hypothesized that one key mode of action by MSCs is through paracrine secretion of soluble factors. MSCs express a range of receptors to recognize inflammatory signals, including tumor necrosis factor–α (TNFα), interferon-γ (IFN-γ), and lipopolysaccharide (LPS) (*4*). Upon inflammatory stimulation, MSCs produce chemokines to recruit immune cells, followed by factors that polarize or differentiate immune cells (*6*). This mode of action is highlighted in regulation of monocytes and their lineages by MSCs (*4*). For instance, nestin$^+$ MSCs in BM secrete CCL2 in response to inflammation in vivo, causing monocytes to emigrate into circulation (*7*). Adoptively transferred MSCs secrete a number of factors to polarize macrophages such as prostaglandin E_2 (PGE_2) and TNFα-stimulated gene 6 (TSG-6), which, in turn, attenuate sepsis (*8*) and regenerate damaged tissues (*9*), respectively. Therefore, understanding how signals from the ECM regulate MSCs to direct monocyte functions will help inform both fundamental insights and previously unidentified strategies to control inflammation and program tissue regeneration (*10*).

Genetic labeling and ablation studies show that some MSC subpopulations are localized like pericytes in the vasculature of the BM (*11*) and contribute to both adipogenic and osteogenic differentiation in vivo (*1*). Other MSC populations are localized more exclusively at the rigid endosteal surface and contribute to bone maintenance and regeneration (*12*). However, vascular and endosteal regions often overlap, and hence, some MSCs contact both regions simultaneously (*2*). Recent studies show that the BM exhibits a diversity of biophysical cues contributed by the ECM. First, the BM shows a range of stiffness (Young's modulus, *E*) from 2 ("soft") to 100 ("stiff") kPa (*13*). In addition, the central regions of the BM may act more like viscoelastic solids than the outer regions of the BM due to fluid transport and exchange through large central vessels (*14*). Advances in biomaterial design have enabled investigators to independently control these biophysical parameters, leading to insights that MSCs are highly sensitive to stiffness (*15*) and stress relaxation (*16*) of matrices, all of which subsequently influence multilineage differentiation. Previous studies show that matrix stiffness regulates secretions of proangiogenic factors (*17*) and factors relevant to hematopoietic recovery (*18*), while substrate dimensionality or topography regulates secretions of factors involved in immunomodulation (*19*). MSCs primed on soft substrates increase survival after radiation-induced hematopoietic failure in vivo (*20*), while a bone-derived scaffold maintains functionality of hematopoietic progenitors when cultured together with MSCs (*21*). However, it remains generally unclear how mechanical cues of the ECM coordinate with biochemical cues during inflammation to program MSC secretomes and, subsequently, to achieve specific functional outcomes. In addition, the relevance of matrix biophysical properties to immunomodulatory functions of MSCs in vivo remains unclear.

By leveraging alginate-based engineered hydrogels, we tested the hypothesis that physiologically relevant matrix stiffness affects the ability of MSCs to modulate monocyte functions under inflammation by paracrine signaling. We show that soft matrix maximizes TNFα-mediated induction of both chemokines and cytokines in MSCs involved in recruitment and differentiation of monocytes, respectively. Through experiments and modeling, we elaborate that soft matrix

[1]Department of Pharmacology and Department of Bioengineering, University of Illinois at Chicago College of Medicine, Chicago, IL, USA. [2]School of Engineering and Applied Sciences, Harvard University, Cambridge, MA, USA.
*Present address: Stanford University School of Medicine, Medical Scientist Training Program, Stanford, CA, USA.
†Corresponding author. Email: mooneyd@seas.harvard.edu (D.J.M.); shinjw@uic.edu (J.-W.S.)

primarily increases clustering of TNF receptors (TNFRs) and binding of TNFα to the cell surface, thereby enhancing activation of nuclear factor κB (NF-κB) to up-regulate downstream genes. Mechanistic studies show that actin polymerization and lipid rafts are involved in mechanosensitive activation of MSCs with TNFα, but not myosin-II contractility. Consistent with these results, we show that human MSCs primed with TNFα in soft matrix enhance in vivo production of human monocytes in marrow of xenografted mice and trafficking of monocytes via CCL2.

RESULTS

Matrix stiffness regulates TNFα-induced gene expression in MSCs

Since BM exhibits diverse mechanical properties (Fig. 1A) (*13*), we used an alginate-based hydrogel system with a conjugated minimal integrin adhesion ligand containing Arg-Gly-Asp (RGD) ("alginate-RGD"). MSCs were encapsulated in the ionically cross-linked alginate-RGD hydrogel so that they could be exposed to a three-dimensional (3D) environment with viscoelastic properties (*16*) typical of marrow ("3D gels") (*14*). By varying ionic cross-linking density, the initial elastic modulus of 3D gels (here, we use the term "matrix stiffness") was tuned as follows: "soft matrix," E = ~2 kPa, and "stiff matrix," E = ~35 kPa (fig. S1A). We first tested whether matrix stiffness regulates constitutive protein secretion by using primary human BM MSCs transduced with *Gaussia* luciferase (~20 kDa). Matrix stiffness does not affect diffusion of *Gaussia* luciferase proteins alone (fig. S1B) and does not alter the ability of genetically engineered MSCs to constitutively produce *Gaussia* luciferase over time (fig. S1C). We then determined whether matrix stiffness affects expression of monocyte regulatory genes in MSCs upon inflammatory stimulation in vitro. TNFα was chosen as the stimulatory cytokine because myeloid cells are known to produce it shortly after inflammation, and it activates MSCs to affect monocyte differentiation and trafficking (*22*). Recombinant TNFα (~50%) diffuses rapidly ($t_{1/2}$ = ~1.2 hours) from the media into 3D gels regardless of their stiffness (fig. S1D). MSCs encapsulated in soft matrix show a higher fold increase in mRNA expression of monocyte regulatory genes, including chemokines [*CCL2* and *CCL7*; monocyte trafficking (*7*)], interleukins [*IL6* and *IL8*; monocyte differentiation (*23*)], and an anti-inflammatory factor [*TSG6* (*9*)] (Fig. 1B), in response to TNFα. Genes that are known to regulate myeloid lineage differentiation (*CSF1*, *2*) and hematopoiesis (*SCF*, *CXCL12*, and *IL11*) also show a similar trend, but with a lower fold increase in gene expression by TNFα (fig. S1E). In contrast, genes involved in angiogenesis (*VEGF* and *ANGPT1*) and macrophage polarization (*IL10*) are up-regulated by TNFα to the same extent regardless of matrix stiffness (fig. S1E). Since *CCL2* and *IL6* show the highest up-regulation by TNFα with sensitivity to matrix stiffness, subsequent studies have focused on these two genes.

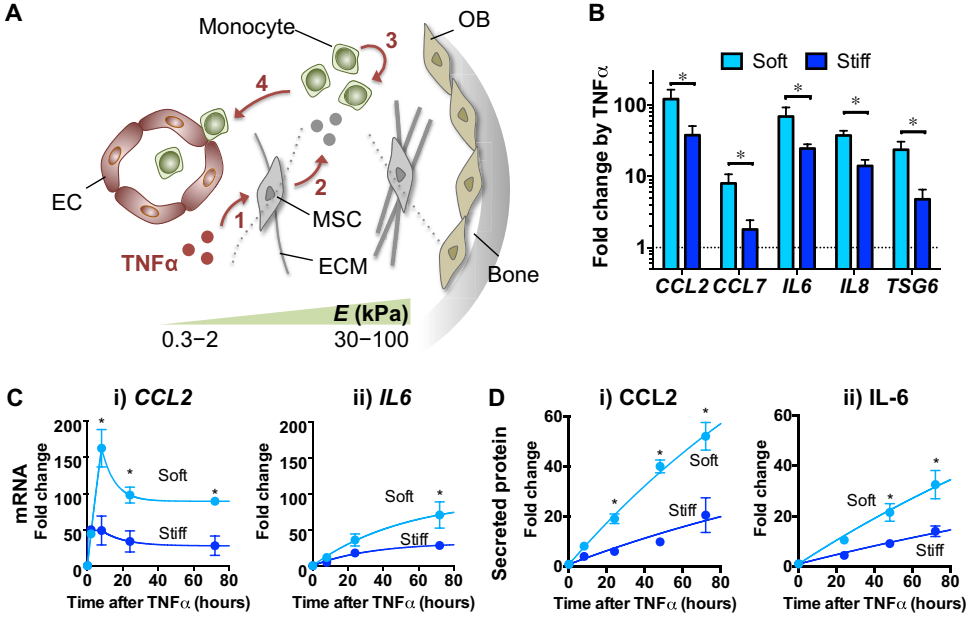

Fig. 1. 3D matrix stiffness regulates expression of TNFα-inducible genes implicated in monocyte functions. (**A**) Schematic showing that matrix stiffness in the bone marrow (BM) microenvironment can potentially influence MSC activation by TNFα to modulate monocyte functions in marrow. The extracellular matrix (ECM) in the central marrow and vascular [endothelial cell (EC)] regions is softer (Young's modulus E = 0.3 to 2 kPa), while that near the bone surface [osteoblast (OB)] is stiffer (E = 30 to 100 kPa) (*13*). Upon inflammation, TNFα could activate MSCs (1) to produce secreted factors (2) that can influence monocyte production (3) and trafficking (4) before systemic distribution. (**B**) Effects of 3D matrix stiffness on TNFα-mediated up-regulation of gene expression in MSCs. MSCs were encapsulated in soft or stiff alginate-RGD 3D hydrogels, incubated for 1 day, and treated with TNFα (100 ng/ml) for 3 days. Transcript levels of the indicated genes were measured by qPCR and normalized against glyceraldehyde 3-phosphate dehydrogenase (*GAPDH*). Fold change by TNFα for each group was then calculated from the untreated control (in log scale). (**C**) Effects of 3D matrix stiffness on mRNA expression kinetics in response to TNFα. (i) *CCL2*: Data from 8 to 72 hours were fitted to standard exponential decay curves. $t_{1/2}$ and plateau for soft: 5.2 hours, 90-fold; stiff: 8.9 hours, 28-fold. (ii) *IL6*: Data were fitted to standard one-phase association curves. $t_{1/2}$ and plateau for soft: 36.5 hours, 95-fold; stiff: 23.2 hours, 33-fold. (**D**) Effects of 3D matrix stiffness on protein secretion kinetics in response to TNFα. Data were fitted to standard one-phase association curves. (i) CCL2: $t_{1/2}$ = 126 hours for both soft and stiff; plateau for soft = 156-fold and for stiff = 61-fold. (ii) IL-6: $t_{1/2}$ = 204 hours for both soft and stiff; plateau for soft = 143-fold and for stiff = 58-fold. Fold change refers to increase over untreated condition. For (B) to (D), paired t test, *P < 0.05 soft versus stiff at each time point (n = 3 donors). Error bars, ±SEM.

Consistent with the results from 3D gels, MSCs plated on the 2D soft gel show higher up-regulation of *CCL2* and *IL6* in response to TNFα than MSCs on the 2D stiff gel or plastic culture (E ~ GPa) (fig. S1F). MSCs in soft matrix show ~150-fold increase in *CCL2* mRNA after 8 hours of TNFα stimulation, followed by stabilization at ~90-fold at 24 to 72 hours (Fig. 1C, i). MSCs in soft matrix show ~3-fold higher *CCL2* mRNA than those in stiff matrix between 8 and 72 hours. Unlike *CCL2*, TNFα gradually increases *IL6* mRNA (Fig. 1C, ii). MSCs in soft matrix show ~3-fold increase in the maximal level of *IL6* mRNA compared with those in stiff matrix. Consistent with the mRNA kinetics, CCL2 protein reaches its half-maximal value faster than IL-6 protein in response to TNFα (Fig. 1D). For both proteins, MSCs in soft matrix show ~2.5-fold higher expression than those in stiff matrix. We chose to use a single MSC donor in the subsequent studies because different MSC donors all exhibited higher expression of CCL2 protein upon TNFα stimulation when encapsulated in soft rather than stiff matrix (fig. S1G). The percentage of viable cells remains >70% in both soft and stiff matrices after culturing for 3 days (fig. S1H). TNFα does not affect the viability of MSCs encapsulated in either soft or stiff matrix (fig. S1H). The effects of matrix stiffness appear to be more selective for TNFα signaling since it does not alter downstream activation of signal transducers and activators of transcription 1 (STAT1) in MSCs by another inflammatory cytokine IFN-γ (fig. S1I). Therefore, matrix stiffness is a key biophysical parameter that regulates TNFα-induced gene expression.

Matrix stiffness regulates TNFα-induced NF-κB activation via TNFR clustering

Since soft matrix enhances TNFα-mediated up-regulation of both CCL2 and IL-6 in a persistent manner (Fig. 1, C and D), we hypothesized that soft matrix enhances activation of NF-κB, a well-known transcription factor of the TNFα signaling pathway (*24*). ML-210B, an inhibitor of IκB kinase β (IKKβ), suppresses TNFα-induced expression of CCL2 and IL-6 at median inhibitory concentration (IC_{50}) 0.5 to 1 μM in both soft and stiff matrices (fig. S2A), confirming that NF-κB activation is required for up-regulation of downstream targets by TNFα. As expected (*24*), the experimental data show that NF-κB becomes maximally activated as early as 10 min after stimulation with TNFα, followed by decrease in 60 min. Consistent with our hypothesis, MSCs in soft matrix show ~1.6-fold higher levels of activated NF-κB in all of the tested time points at $t \geq 10$ min (Fig. 2A and fig. S2B).

We developed a parsimonious mathematical model using a minimal number of functions and variables to gain further insights into how matrix stiffness may regulate NF-κB activation by TNFα. Because NF-κB activation occurs in a pulse-like manner (*24*) (Fig. 2A), we devised a set of ordinary differential equations describing an incoherent type-1 feed-forward loop (I1-FFL) (*25*), a simple network motif where activation of TNFRs not only drives NF-κB activation through the IKK followed by IκB degradation (*24*) but also recruits putative factors that inhibit NF-κB activation (fig. S2C, i). From this model, the governing equation describing the NF-κB activation kinetics under I1-FFL can be derived analytically (fig. S2C, ii, and Supplementary Materials). Fitting the data to the equation (Fig. 2A) suggests that matrix stiffness primarily changes the maximal level of activated NF-κB but not the other parameters of the I1-FFL model (fig. S2D and Supplementary Materials).

Matrix stiffness may affect the maximal level of activated NF-κB by tuning either the constitutive activation rate of NF-κB or dose response of TNFα binding to its receptors (Supplementary Materials). The basal level of activated NF-κB in the absence of TNFα remains the same when MSCs are encapsulated in either soft or stiff matrix (fig. S2E), suggesting that the constitutive level of activated NF-κB is less likely influenced by matrix stiffness. Therefore, we tested whether matrix stiffness regulates the TNFα dose response under continuous treatment for 3 days. While soft matrix increases the maximum response of *CCL2* and *IL6* mRNA expression, matrix stiffness does not affect the dose required for the half-maximum response (i.e., TNFα potency) (Fig. 2B). Since matrix stiffness does not alter total TNF receptor 1 (TNFR1) expression (fig. S2F), the data suggest that matrix stiffness may regulate surface receptor clustering or density, but not intrinsic receptor affinity or conformation. To further investigate this idea, we performed confocal imaging analysis of hydrogel-encapsulated live MSCs that overexpress TNFR1 fused with yellow fluorescent protein (YFP). We labeled gel-encapsulated live MSCs with a cell-tracking dye to label the cytoplasmic compartment so that TNFR1-YFP in the cell surface and the cytoplasmic compartments could be distinguished by image processing (fig. S3A and Materials and Methods). As predicted, the cluster size of cell surface TNFR1-YFP is generally larger when MSCs are encapsulated in soft than stiff matrix and cultured for 1 day even in the absence of TNFα (Fig. 2C, i and ii). In response to TNFα, MSCs in soft matrix show ~2-fold increase in the cluster size of surface TNFR1-YFP (Fig. 2C, ii) and ~2-fold decrease in the number of surface TNFR1-YFP clusters per cell (Fig. 2C, iii). Since the level of surface TNFR1-YFP relative to that of the total TNFR1-YFP remains unchanged by TNFα (Fig. 2C, iv), the results suggest that TNFR1-YFP undergoes consolidation by lateral clustering in response to TNFα when MSCs are in soft matrix. In contrast, TNFα does not influence TNFR1-YFP clustering when MSCs are in stiff matrix (Fig. 2C). The same phenotypes are also observed with HeLa cells (fig. S3B), which are known to express $\alpha_5\beta_1$ integrins (*26*) and undergo TNFR1 clustering (*27*), suggesting that the effect of matrix stiffness on TNFR1 clustering in response to TNFα may be generalizable to other adherent cells. Thus, soft matrix is an enabling environment for MSCs to respond to TNFα by TNFR clustering, thereby facilitating activation of downstream NF-κB and subsequent gene expression.

Matrix stiffness regulates TNFα binding to cell surface via actin polymerization and lipid rafts

Since actin polymerization and contractility are important for the ability of cells to sense matrix stiffness (*15*), we tested whether these processes are required for mechanosensitive activation of MSCs by TNFα. Consistent with increased TNFα-induced TNFR1 clustering in soft matrix (Fig. 2C), more TNFα binds to MSCs in soft matrix than in stiff matrix (Fig. 3A). While inhibition of actin polymerization by latrunculin A suppresses TNFα ligand binding when the hydrogel is soft, inhibition of myosin-II contractility by blebbistatin does not affect TNFα ligand binding (Fig. 3A). Consistent with these results, short-term treatment of latrunculin A is sufficient to disrupt up-regulation of CCL2 mRNA by TNFα selectively in the soft hydrogel (Fig. 3B). However, blebbistatin does not alter CCL2 mRNA up-regulation by TNFα (Fig. 3C). Thus, the results suggest that actin polymerization, but not myosin-II contractility, mediates enhanced responsiveness of MSCs to TNFα in soft matrix.

To understand what other mechanisms may be involved in regulating mechanosensitive TNFα activation, we explored roles of lipid rafts, which are known to facilitate receptor clustering (*28*) and to

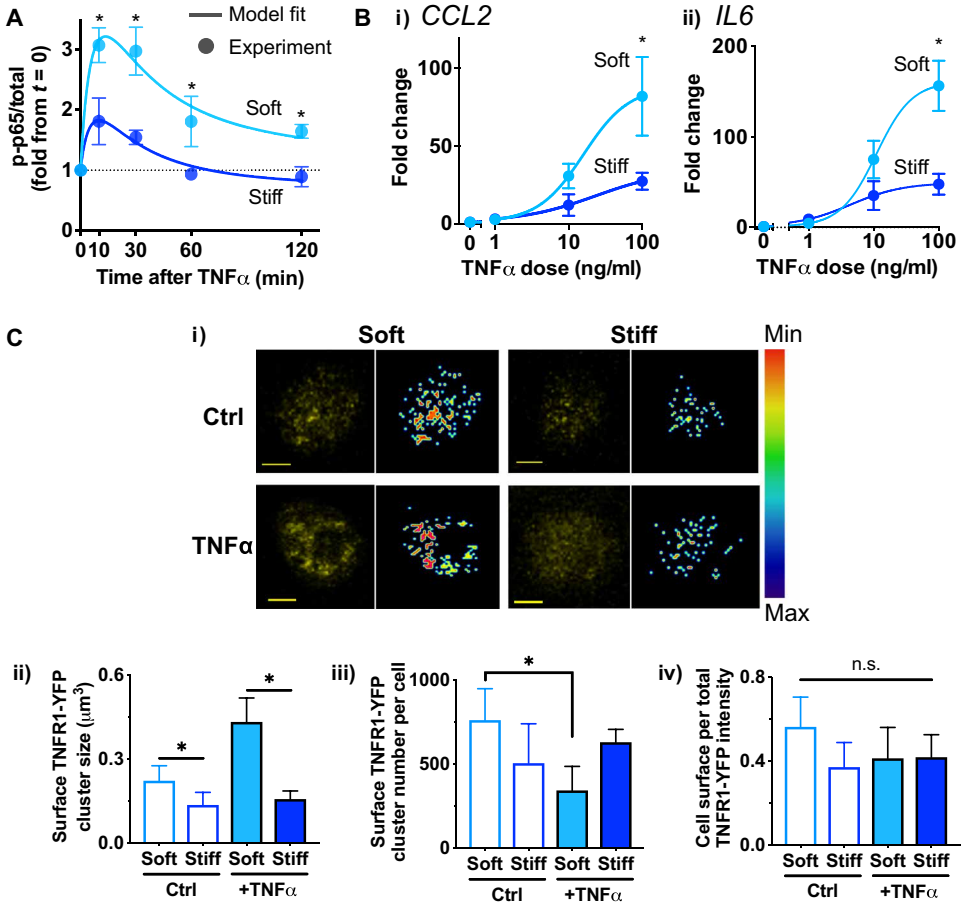

Fig. 2. Soft matrix increases NF-κB activation by facilitating TNFR1 clustering in response to TNFα. (**A**) NF-κB activation kinetics of MSCs in soft or stiff 3D gels in response to TNFα (100 ng/ml) evaluated by p65 phosphorylation at Ser^{536} (p-p65). The experimental results from soft and stiff alginate hydrogels are fitted to the I1-FFL–based model derived analytically ($R^2 > 0.8$; Supplementary Materials). (**B**) Dose-response curves of TNFα to up-regulate mRNA expression in soft and stiff alginate-RGD hydrogels after the 3-day continuous treatment. (i) *CCL2*: IC_{50} and maximum fold increase for soft = 17 μM, 88-fold, and for stiff = 20 μM, 35-fold. (ii) *IL6*: IC_{50} and maximum fold increase for soft = 9 μM, 160-fold, and for stiff = 7 μM, 50-fold. *$P < 0.05$, paired *t* test. For (A) and (B), paired *t* test, *$P < 0.05$ soft versus stiff at each time point or dose ($n = 3$ experiments). Error bars, ±SEM. (**C**) Cell surface distribution and clustering of TNFR1-YFP in MSCs encapsulated in soft or stiff 3D gels. (i) Representative confocal images for each group showing maximum projection of TNFR1-YFP (left, yellow) and cell surface TNFR1-YFP after filtering (right, scale bar, min: 0, max: 255; fig. S2H). (ii) Cluster size of TNFR1-YFP on the cell surface. (iii) Cluster number of TNFR1-YFP per cell. (iv) Cell surface per total TNFR1-YFP intensity. $P < 0.05$ one-way Brown-Forsythe and Welch ANOVA for (ii) and (iii) with Dunnett T3 multiple comparisons test, *$P < 0.05$ ($n \geq 15$ cells from two experiments). Error bars, ±SD. n.s., not significant.

recruit TNFR1 for NF-κB activation by TNFα (*29*). Lipid rafts are sensitive to biophysical stimuli as they rapidly disappear when intracellular tension is high (*30*). Consistent with this notion, MSCs in the soft matrix exhibit a higher phospho-Y14 level of caveolin-1 than the stiff matrix in the absence of TNFα, indicating higher lipid raft activation in soft matrix (Fig. 3D). The expression level of caveolin-1 remains similar after MSCs are cultured in soft and stiff matrices for 1 day (Fig. 3E). Disrupting lipid rafts with nystatin reduces TNFα binding to MSCs in soft, but not stiff, matrix (Fig. 3F). Consistently, treating MSCs with nystatin decreases TNFα-mediated expression of *CCL2* in MSCs encapsulated in the soft matrix (Fig. 3G).

To further understand how actin polymerization and lipid rafts mediate TNFR1 clustering as a function of matrix stiffness, MSCs overexpressing both TNFR1-YFP and LifeAct–red fluorescent protein (RFP) that binds to F-actin (*31*) were studied. F-actin is greater in MSCs in stiff matrix than MSCs in soft matrix (fig. S4A). Most TNFR1-YFP cluster on the cell surface at regions of high F-actin (fig. S4B). Dual expression of TNFR1-YFP and LifeAct-red reveals a similar effect of matrix stiffness on TNFR1-YFP clustering upon TNFα stimulation as in Fig. 2C (fig. S4C). Consistent with the results in Fig. 3F, nystatin inhibits TNFα-induced clustering of TNFR1-YFP on the cell surface in soft matrix (fig. S4C). F-actin colocalized with TNFR1-YFP near the cell surface is increased in soft matrix, but not stiff matrix, in response to TNFα; this effect is abolished by nystatin (fig. S4D). Concomitantly, F-actin is decreased near the cell surface in regions where TNFR1-YFP clusters are not present, when MSCs in soft matrix are treated with TNFα—nystatin also reverses this effect (fig. S4E). Thus, soft matrix enables lipid rafts to enhance TNFR1 clustering upon TNFα stimulation by mediating redistribution of actin polymerization (Fig. 3H).

Matrix stiffness regulates MSC paracrine modulation of monocyte production and chemotaxis

Since matrix stiffness mediates TNFα-induced production of cytokines implicated in monocyte differentiation and polarization (Fig. 1B), we tested whether matrix stiffness influences the ability of MSCs to

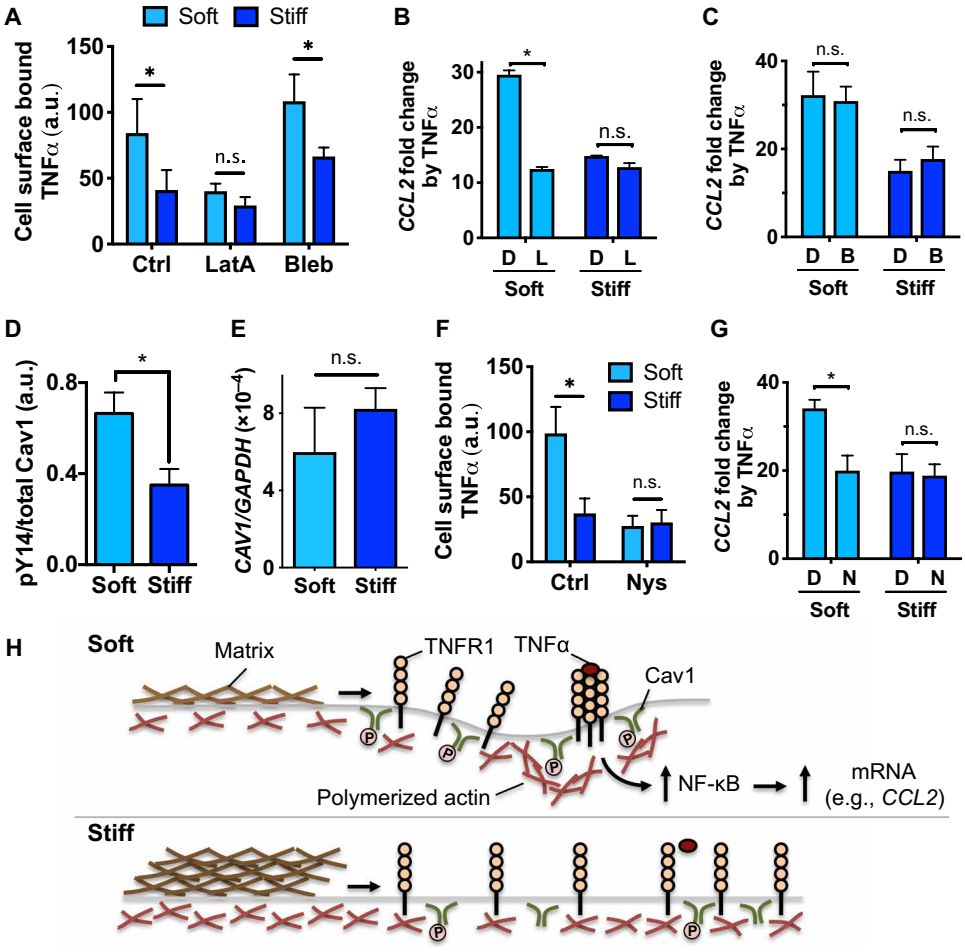

Fig. 3. Actin polymerization and lipid rafts mediate responsiveness of MSCs to TNFα in soft matrix. (**A**) TNFα binding to MSCs in soft or stiff 3D gels in the presence of DMSO (Ctrl), latrunculin A (LatA, 0.25 μM), or blebbistatin (Bleb, 10 μM) for 3 hours. $P < 0.05$ two-way ANOVA with Sidak's multiple comparison test, $^*P < 0.05$ ($n = 3$ experiments). (**B**) Effects of inhibiting actin polymerization on TNFα-induced *CCL2* mRNA expression. MSCs in soft or stiff 3D gels were preincubated with DMSO ("D") or latrunculin A ("L") for 1 hour, treated with or without TNFα in the presence of the drugs for 2 hours, followed by washout and incubating in media for 1 day prior to qPCR. (**C**) Effects of inhibiting myosin-II contractility on TNFα-induced CCL2 protein expression. Gel-encapsulated MSCs were treated with TNFα in the presence of DMSO ("D") or blebbistatin ("B") in the same manner as (B). (**D**) Phosphorylation level of caveolin-1 (Cav1) at Tyr14 in MSCs after 1 day of encapsulation in soft or stiff 3D gels. (**E**) Gene expression of *CAV1* relative to *GAPDH* measured by qPCR after culturing MSCs in soft or stiff 3D gels for 1 day. (**F**) TNFα binding to MSCs in soft or stiff 3D gels in the presence of DMSO (Ctrl) or nystatin (Nys, 50 μM) for 2 hours, followed by washout and incubating in media for 1 day prior to qPCR. (**G**) Effects of inhibiting lipid rafts on TNFα-induced *CCL2* mRNA expression in the presence of DMSO ("D") or nystatin ("N") in the same manner as (B). For (B) to (G), $^*P < 0.05$, paired *t* test; $n = 3$ experiments; and error bars, ±SEM. (**H**) Model of actin polymerization and lipid rafts in mediating matrix stiffness–dependent binding of TNFα to the cell surface. In soft matrix, lipid rafts mediate redistribution of actin polymerization to facilitate clustering of TNFR1 in response to TNFα. In contrast, stiff matrix impedes this process, thereby impairing TNFR1 clustering and TNFα binding. a.u., arbitrary unit.

affect hematopoiesis in vitro by conducting coculture experiments. After priming human MSCs in different culture environments with or without TNFα, they were retrieved and cocultured with cord blood $CD34^+$ hematopoietic and stem progenitor cells (HSPCs) in the viscous alginate-RGD fluid without cross-linking, which mimics the known viscosity value of blood or marrow (*32*) (fig. S5A, i). Most MSCs remain viable after a 4-day culture in the alginate-RGD fluid (fig. S5A, ii). Multicolor flow cytometry was used to quantify different hematopoietic subpopulations as described (*33*, *34*). While MSCs do not affect early HSPCs, multipotent progenitors, and common myeloid progenitors, they generally increase granulocyte/monocyte progenitors and differentiated $CD14^+$ monocytes—in particular, MSCs primed in soft matrix with TNFα shows the highest number of differentiated monocytes compared with MSCs primed in stiff matrix or on 2D plastic culture (fig. S5B). To confirm these results in vivo, we established human hematopoiesis prior to MSC delivery by injecting cord blood $CD34^+$ cells in the nonobese diabetic (NOD)/severe combined immunodeficient (SCID)/IL-$2\gamma^{-/-}$ (NSG) mice. In this model, human myeloid lineage becomes detectable after 14 days (*35*). After 10 days of transplanting cord blood $CD34^+$ cells, we encapsulated human MSCs in soft or stiff 3D alginate-RGD hydrogels, cultured for 1 day, and treated with or without TNFα for 3 days. Alginate lyase was then used to retrieve MSCs from gels, followed by injection of MSCs into the right tibial BM after 14 days of cord blood $CD34^+$ transplantation (Fig. 4A). Phosphate-buffered saline (PBS) was delivered into the left tibial BM as a control. Four days after delivering MSCs, the total percentage of human $CD45^+$ cells in marrow is 20 to 30% on average with no significant difference

between the tibias or across the experimental groups (fig. S6A). Previous studies show that three monocyte subsets exist in humans based on expression of CD14 and CD16 during differentiation (*36*). Consistent with these studies, we show that the majority of the monocytes in marrow across the tested groups are classical ($CD14^+CD16^-$), while ≤5% of $CD14^+$ cells (or ≤1% of total human $CD45^+$ cells) are intermediate ($CD14^+CD16^+$). Nonclassical ($CD14^-CD16^+$) monocytes are not detectable in the NSG mice, as shown previously (*37*). Delivery of TNFα-primed MSCs from either soft or stiff matrix leads to ~3-fold higher percentage of classical monocytes in the cell-injected tibia compared with that of unprimed MSCs or PBS control (Fig. 4B, i). The PBS-injected tibia also shows increased classical monocytes upon delivery of TNFα-primed MSCs from soft, but not stiff, matrix to the other tibia (Fig. 4B, i). In addition, TNFα-primed MSCs from the soft matrix increase percentage of intermediate monocytes in the cell-injected tibia to the known physiological level (*38*) (1 to 2% of $CD14^+$ cells, or 0.2 to 0.4% of total human $CD45^+$ cells) (Fig. 4B, ii). Intermediate monocyte levels are also increased in the PBS-injected left tibia when TNFα-primed MSCs from the soft matrix are delivered to the right tibia (Fig. 4B, ii). Live imaging via IVIS shows that MSCs remain localized within the cell-injected tibia after delivery for at least 4 days (Fig. 4C). Since the effect of MSCs on monocyte production in a distal BM compartment is not seen when they are stimulated with TNFα in 3D stiff matrix, it is less likely that the effect will be seen with MSCs primed on 2D matrices or plastic culture (fig. S1F) due to an order of magnitude lower level of up-regulation in monocyte regulatory factors as compared with MSCs in 3D gels. Together, the results show that ex vivo priming of MSCs with TNFα in soft matrix, but not stiff matrix, enhances monocyte production in both local and distal BM compartments in vivo.

Once monocytes are generated, they need to be recruited to blood vessels so that they can enter circulation. Since CCL2 secreted from MSCs plays a critical role in this process (*7*), we tested whether matrix stiffness regulates the ability of MSCs to recruit monocytes and other blood lineages. $CD14^+$ monocytes (~2.5%) from human peripheral blood mononuclear cells migrate through 3-μm pores when the conditioned media from human MSCs are applied—priming human MSCs in the soft matrix with TNFα prior to collecting the media enhances $CD14^+$ cell migration to ~10%, while doing so in the stiff matrix or on 2D plastic culture shows no effect (Fig. 4D, i, and fig. S6B). The neutralizing antibody against CCL2 is sufficient to eliminate the phenotype (Fig. 4D, ii). Migration of lymphocyte lineages is generally low (<2.5%) toward the conditioned media from MSCs on 2D plastic culture, but priming with TNFα increases migration of $CD4^+$ and $CD8^+$ T cells and $CD56^+$ natural killer cells to ~15%, while that of $CD19^+$ B cells remains ~2.5% (fig. S6B).

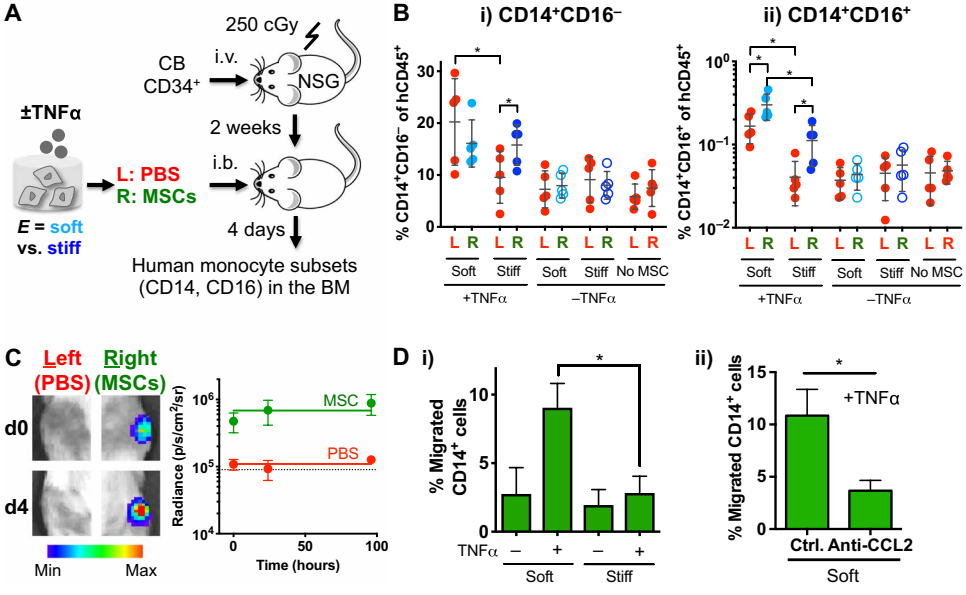

Fig. 4. Soft matrix promotes the ability of MSCs to produce and recruit monocytes upon TNFα stimulation. (**A**) Experimental scheme. Sublethally irradiated (250 cGy) NSG mice were injected intravenously (i.v.) with 20,000 human cord blood HSPCs per 20 g of mouse. After 2 weeks, MSCs that were cultured in soft or stiff gels for 1 day followed by ±TNFα treatment (100 ng/ml) for three additional days were retrieved and delivered to the right (R) tibia by an intrabone (i.b.) route, while the left (L) tibia was delivered with PBS. After 4 days, both tibias were analyzed for human monocyte subsets. (**B**) Percentage of (i) classical ($CD14^+CD16^-$) and (ii) intermediate ($CD14^+CD16^+$) human monocytes in tibias. $P < 0.05$, two-way ANOVA with Sidak's multiple comparison test, $^*P < 0.05$. $n = 5$ recipients from two independent experiments. (**C**) MSCs remain localized in one tibia after intrabone delivery to NSG mice. Firefly luciferase–transduced MSCs were delivered in the right tibia, while PBS was injected in the left tibia, followed by IVIS imaging over 4 days. Left: Representative images at days 0 and 4 after MSC delivery. Scale bar, radiance (p/sec/cm^2/sr, min: 1 M, max: 15 M). Right: Quantification of radiance signals over 4 days. The signal from the left tibia remains at the background level (~90,000, dotted line), while that from the right tibia remains ~10-fold higher over the 4 days. (**D**) TNFα-treated MSCs in soft matrix increase migration of human peripheral blood $CD14^+$ monocytes via secretion of CCL2. MSCs in soft or stiff alginate hydrogel were treated with TNFα (100 ng/ml) for 1 day prior to washout and collection of the media for 1 day for the Transwell migration assay. (i) The extent of $CD14^+$ migration under chemotactic gradient through 3-μm pores for 3 hours. $P < 0.05$ from one-way ANOVA with Tukey's post hoc test, $^*P < 0.05$ ($n = 3$ experiments). (ii) CCL2 is required for increased chemotaxis of $CD14^+$ cells by the media from TNFα-treated MSCs in soft matrix. The media were treated with a neutralizing antibody against CCL2 (anti-CCL2) or isotype control (ctrl) for 3 hours prior to the Transwell assay. $^*P < 0.05$, paired *t* test ($n = 3$ experiments). All error bars for both (i) and (ii), ±SEM.

In contrast, 5 to 25% of lymphocytes are migrated toward the conditioned media from MSCs cultured in soft or stiff matrix even in the absence of TNFα, while TNFα does not further enhance migration (fig. S6C). These results suggest that, in addition to enhancing production of monocytes, soft matrix increases the ability of MSCs to selectively recruit them upon TNFα activation.

DISCUSSION

Stromal cells play important roles in regulating immune cells across different tissues. Previous studies have mostly focused on how a variety of biochemical cues enable stromal cells to modulate immune cells (*4*, *6*). Here, we show that physiological relevant mechanical cues regulate the sensitivity of BM MSCs to an inflammatory cytokine TNFα and their subsequent ability to modulate monocytes. Presence of TNFα has been closely linked to controlling monocyte turnover and functions. Myeloid rather than lymphoid cells were shown to be mainly responsible for in vivo production of TNFα during inflammation (*39*), which in turn regulates in vivo survival and functions of monocytes (*40*). CCL2-producing stromal cells in vivo are strategically localized near the vasculature in the BM to recruit and egress monocytes during inflammation (*7*). Consistent with this notion, our results show that matrices mimicking stiffness of the soft vascular niche lead to higher production of monocyte regulatory factors in MSCs upon TNFα stimulation than those mimicking the more rigid endosteal niche (Fig. 1). Thus, the results suggest the important role of biophysical cues in the BM in modulating TNFα-mediated production of monocyte regulatory factors in MSCs.

The activation kinetics of NF-κB in response to TNFα has been extensively studied with quantitative modeling (*24*). An incoherent feed-forward loop from competitive binding between NF-κB and an inhibitory transcription factor to promoter regions allows cells to tune TNFα-induced transcription in response to fold change rather than absolute abundance of activated NF-κB (*41*). However, our analysis suggests a possibility that an incoherent feed-forward loop may also play an upstream role in the NF-κB pathway when TNFα activates and clusters TNFRs (fig. S2C). The exact identity of the putative inhibitory components in the loop remains to be elucidated, but previous studies suggest potential candidates, including wild-type p53-induced phosphatase 1 (WIP1) (*42*) and protein phosphatase 4 regulatory subunit 1 (PP4R1) (*43*). While soft matrix persistently increases NF-κB activation by ~1.6-fold compared with stiff matrix after 10 min of TNFα stimulation (fig. S2B), this effect appears to be amplified downstream as shown by more than twofold higher up-regulation in target genes (Fig. 1) and paracrine monocyte production and migration (Fig. 4). Future studies will help elucidate how the effect of matrix stiffness on TNFα activation can result in amplified downstream effects.

Our studies point to potential mechanisms by which matrix stiffness regulates TNFα ligand binding to the cell surface. A previous study shows that EDTA decreases binding of biotinylated LPS to monocytes after 60 min of incubation (*44*). Here, EDTA was used to rapidly digest alginate gels so that encapsulated MSCs can be retrieved in ~5 min prior to analyzing TNFα ligand binding on the cell surface (Materials and Methods). While this short time frame of EDTA treatment may less likely affect TNFα binding to TNFR, fluorescently tagged TNFα may be used in future studies to directly visualize TNFα binding to MSCs in gels. Consistent with this idea, confocal imaging of live MSCs in intact gels shows that soft matrix increases surface TNFR1 clustering (Fig. 2C). Previous studies show that cells cultured on soft matrices internalize integrin β_1 receptors through lipid rafts (*45*) and integrin β_3 receptors through clathrin (*46*), both in a myosin-II–dependent manner. Cells on less contractile 2D geometry were recently shown to increase TNFα-induced activation of NF-κB by decreasing myosin-II–mediated contractility (*47*). However, our results suggest a distinct regulatory mode, where matrix stiffness modulates cell sensitivity to an inflammatory signal in a myosin-II independent but actin polymerization– and caveolae–dependent manner (Fig. 3). Actin polymerization and caveolae may synergize with each other to facilitate TNFR clustering and TNFα binding in soft matrix, since polymerized actin is known to stabilize the neck part of caveolae to concentrate surface receptors (*28*). As the ECM becomes stiffer, actin polymerization may instead be used to increase cortical tension (*15*, *48*), which is shown to decrease caveolae formation (*30*). Elucidating mechanisms behind how actin polymers and lipid rafts interact as a function of matrix stiffness will be important to further understand roles of matrix stiffness in regulating surface receptor dynamics and its implications in MSC functions.

In addition to the NF-κB pathway, matrix stiffness can potentially influence other TNFα-activated downstream signaling pathways, including mitogen-activated protein kinases (e.g., p38 and JNK) and caspases (*49*). In particular, JNK and caspases-8 are required to induce apoptosis in response to TNFα in immune cells, while NF-κB activation is known to inhibit cell death (*50*). However, our results show that TNFα does not affect the viability of MSCs (fig. S1H). TNFR1 can activate both survival and apoptotic pathways depending on interactions with distinct adaptor proteins, such as TNFR-associated death domain protein (TRADD) and Fas-associated death domain (FADD) (*49*). Thus, future studies may help identify adaptor proteins that bind to TNFR1 as a function of matrix stiffness and how this process can selectively affect downstream signaling.

While TNFα directly acts on HSCs to regulate hematopoiesis under both baseline and inflammatory conditions (*51*), our results suggest that stromal cells together with matrix stiffness may also contribute to monocyte generation from hematopoietic progenitors in response to TNFα. The NSG model used in this study shows a transient increase in monocyte subpopulations between 2 and 3 weeks after transplantation of human hematopoietic progenitors (*37*). Since injection of human TNFα-primed MSCs from soft matrix leads to the physiological level of human intermediate monocytes (Fig. 4B, ii), this model can potentially be used to study clinical relevance of this population, which was previously implicated in liver regeneration (*38*). While the NSG model is appropriate to study the short-term effect of MSCs on human monocyte production, other emerging models, such as mice engineered to express human cytokines (*37*), can be used in future studies to study more long-term effects. In addition, genetic knockout strategies to delete TNFRs specifically in MSCs in situ could help validate their contribution to controlling monocyte turnover.

The approach presented here can broadly serve as a platform to prime MSCs with a combination of biophysical and biochemical cues and deliver them orthotopically to the BM to control immune cell turnover in vivo. Different routes of administration have been explored to test therapeutic efficacy of MSCs, including intravascular routes, which have been pursued by ~40% of the clinical trials (*52*). The intravascular routes are commonly used to deliver mononuclear blood cells as in hematopoietic transplantation, since they can readily

deform and squeeze through confined spaces, including capillaries (*53*). In contrast, MSCs are larger and more rigid than blood cells, hindering their trafficking through small pores (*54*). Consistent with these observations, MSCs delivered intravascularly are known to be localized primarily to the lungs due to microembolism and to be cleared within 24 hours (*5*) without successful engraftment in marrow (*55*). Since monocyte lineages play a role in clearance, it is possible that phagocytosis of MSCs that fail to engraft after intravascular injection can potentially affect the phenotype of monocytes or macrophages as suggested (*56*). In contrast, our results inform a fundamentally distinct strategy where delivering MSCs via the intrabone route not only maintains their in vivo residence in local marrow but also encourages production of monocytes from human hematopoietic progenitors in vivo. Generalizability of this strategy will depend on in vivo demonstration with multiple MSC donors in the future. In addition, it will be important to successfully retrieve cells from gels while maintaining viability and functionality after retrieval. While alginate lyase used in this study is known to be orthogonal to mammalian cells because they do not express alginate (*57*), introducing more natural mechanisms in hydrogel design such as protease degradable sequences (*58*) can be useful to retrieve cells without a need to use an external degradation mechanism. MSCs in soft hydrogel maintain higher CCL2 expression for 1 day even after transiently stimulated with TNFα for 2 hours (Fig. 3), suggesting a possibility that MSCs can potentially maintain their secretomes even after ex vivo priming is complete. However, strategies to locally specify insoluble biophysical cues around cells in vivo, such as microfluidic thin gel coating (*59*), can help present MSCs with predefined biochemical and matrix biophysical cues in a continuous manner in vivo. Since monocytes generated from the BM contribute to the pool of tissue macrophages in various disease conditions including tissue damage and fibrosis (*10*), the ability to systematically control monocyte turnover, as exemplified by our approach, may help inform therapeutic strategies for these diseases.

MATERIALS AND METHODS

MSC isolation and expansion

MSCs were derived by plastic adherence ("passage 0") of mononucleated cells from human BM aspirate donors (Lonza). After plastic adherence for 3 days, nonadherent cells were washed out, and adherent cells were cultured at 37°C in 5% CO_2 in the MSC medium: α-minimal essential medium (αMEM) supplemented with 20% fetal bovine serum (Atlanta Biologicals), 1% penicillin/streptomycin (P/S; Thermo Fisher Scientific), and 1% GlutaMAX (Thermo Fisher Scientific). After reaching 70 to 80% confluence at around 10 to 14 days, cells were split and expanded in the MSC medium. MSCs became >80% confluent within a week after ~500,000 cells were plated on a 175-cm^2 flask. No difference was observed among tested donors in terms of the rate of proliferation. Passage numbers up to "4" or total culture day from initial plastic adherence up to 43 were used for experiments. After this passage number, MSCs undergo slower cell proliferation and were not used for experiments.

Alginate-based hydrogels for cell culture

Alginate from brown algae was purchased from a commercial vendor (FMC BioPolymer). Sodium alginate with a high molecular weight (LF200) and a low molecular weight (LF10/60) was dialyzed against deionized water for 3 days (molecular weight cutoff of 3500 Da), treated with activated charcoal, sterile filtered, and lyophilized. Before encapsulation, lyophilized alginate was reconstituted in FluoroBrite Dulbecco's modified Eagle's medium (DMEM) at 3 to 4% (w/v) as a stock solution. For LF200 alginate, an RGD peptide (GGGGRGDSP, Peptides International) was conjugated using carbodiimide chemistry at 20 RGD peptides per alginate chain [or ~750 μM RGD in 1% (w/v) alginate]. The coupling efficiency was previously characterized (*48*). For gelation, 1% (w/v) LF10/60 alginate was combined with 1% (w/v) LF200-RGD alginate [total 2% (w/v)], so that all hydrogels contain the same amount of RGD ligand, and rapidly mixed with DMEM containing the appropriate concentration of calcium sulfate. The mixed solution was deposited between two glass plates with 1-mm thickness. After 1.5 hours, hydrogels were punched into discs. For 2D hydrogels, discs were placed in ultralow attachment plates (Corning), so that cells could be seeded selectively on gels but not on plastic surface. For 3D hydrogels, cells were mixed with alginate prior to gelation. Cells on or in gels were incubated in FluoroBrite DMEM (Thermo Fisher Scientific) supplemented with 1% P/S and 1% GlutaMAX.

Mechanical characterization

To determine Young's modulus (E) of hydrogels, a gel disc of 5 mm by 1 mm was first placed onto a polydimethylsiloxane mold on a glass slide and immersed in a drop of DMEM. The slide was then placed in an MFP-3D system (Asylum Research) to perform atomic force microscopy analysis with silicon nitride cantilevers (Bruker Model MLCT). A spring constant of the cantilever was determined from thermal fluctuations at room temperature (RT) (20 to 40 mN/m). The cantilever was brought toward the hydrogel surface at 1 μm/s and indented on the surface until it reached the trigger voltage (0.5 V), followed by retraction. Force-indentation curves were fitted using the Hertzian model with a pyramid indenter.

Establishing MSCs that express exogenous genes

To introduce firefly or *Gaussia* luciferase in MSCs, premade lentiviral particles containing mCherry–internal ribosomal entry site (IRES)–Firefly luciferase or cyan fluorescent protein–IRES-Gaussia luciferase were purchased from the Mass General Hospital Vector Core. MSCs were incubated with viral particles for 2 days. Fluorescent MSCs were then isolated by fluorescence-activated cell sorting and expanded for further analysis.

Quantification of viable and dead cells

Hydrogels with encapsulated cells were digested with alginate lyase (3.4 mg/ml; Sigma-Aldrich) in Hanks' balanced salt solution (HBSS) for 30 min at 37°C. The digested solutions were directly added to HBSS that contains calcein AM (1:2000; Biotium), ethidium bromide (1:2000; Thermo Fisher Scientific), and a predefined number of allophycocyanin (APC) beads (BD). After incubation at RT for 10 min, the samples were analyzed by flow cytometry.

Gene expression analysis

At a desired time point, culture media were removed, and gel discs containing 3D encapsulated cells were washed with HBSS twice. Gel digestion and cell lysis were done simultaneously using 50 mM EDTA in ribonuclease (RNase)–free water for less than 1 min. The samples were then directly added to TRIzol (Thermo Fisher Scientific). Chloroform (200 μl) was added per 1 ml of TRIzol to perform phase separation, followed by centrifugation for 15 min at 12,500 rpm,

4°C. The top layer was collected to a new tube, and RNA was precipitated with 250 µl of isopropanol and 250 µl of solution of 0.8 M sodium citrate and 1.2 M sodium chloride for at least 15 min at 4°C. Samples were then centrifuged at 12,500 rpm for 15 min at 4°C. The supernatant was removed, and the precipitated RNA was washed with 75% EtOH, followed by centrifugation for 5 min at 7500 rpm, 4°C. EtOH was then removed, and the purified RNA was resuspended in 15 µl of RNase-free water. RNA concentration was quantified by the NanoDrop spectrophotometer. Complementary DNA (cDNA) was reverse transcribed by SuperScript-III reverse transcriptase (Thermo Fisher Scientific). Quantitative polymerase chain reaction (qPCR) was performed in the ViiA7 qPCR system with Power SYBR Green master mix (Applied Biosystems). For each qPCR experiment, samples were analyzed in triplicates with 50 ng of cDNA per well. Relative gene expression was computed by the delta-delta Ct method by comparing Ct values to reference gene (*GAPDH*). See table S1 for the list of primers for qPCR.

Measuring levels of secreted proteins

To determine constitutive secretion of *Gaussia luciferase* from engineered MSCs, collected media were diluted ~100-fold and added to a white, opaque 96-well plate. The sample (10 µl) was mixed with 100 µl of coelenterazine h substrate (10 µg/ml; Biotium) in PBS immediately prior to measurement by using a luminometer that can programmatically inject the substrate (BioTek). Photon counts were acquired for 10 s. To determine levels of secreted human CCL2 and IL-6 in culture media, a sandwich enzyme-linked immunosorbent assay was used as described by the manufacturer's (Peprotech) protocol. Briefly, samples were diluted ~10-fold and incubated overnight in a 96-well plate (Nunc MaxiSorp, Thermo Fisher Scientific) coated with primary capture antibody. Samples were then incubated with primary detection antibody for 2 hours, followed by secondary antibody conjugated to horseradish peroxidase (HRP) for 30 min. Samples were washed out between each step with PBS with 0.05% Tween 20. At the final step, the HRP substrate, 3,3′,5,5′-tetramethylbenzidine (TMB), was added to detect HRP activity. After developing for 10 to 15 min, the equal volume of 1 M HCl was added to neutralize the reaction. A plate reader (PHERAstar) was used to read absorbance at 450 nm. The media incubated without cells were used to determine background signals. The total protein amount of each sample was normalized to total viable cell number.

Characterization of NF-κB activation kinetics

After culturing cells in gels for 1 day, recombinant TNFα (100 ng/ml; Peprotech) was added. At indicated time points, cells were rapidly retrieved from alginate hydrogels by adding 30 mM EDTA in DMEM with 1% bovine serum albumin (BSA) for 5 min on ice. During this process, dead cells were labeled with the LIVE/DEAD fixable violet dead cell stain (1:1000; Thermo Fisher Scientific). Cells were then washed out with DMEM with 1% BSA and fixed with 4% paraformaldehyde in HBSS at RT for 10 min. After washing two times with PBS/0.1% BSA, cells were stained with either phospho–NF-κB p65 (Ser^{536}) (93H1) or total NF-κB p65 (D14E12) antibody (both from Cell Signaling Technology) at 1:100 dilution in the staining buffer (HBSS/0.1% saponin/0.1% BSA) at RT for 2 hours. They were then washed out once with the staining buffer and incubated with a secondary antibody (donkey Alexa 647 anti-rabbit, Thermo Fisher Scientific) for 30 min at RT, followed by washing out and resuspension in HBSS. Flow cytometry analysis was done using LSRFortessa (BD). The sample incubated with the isotype control [rabbit immunoglobulin G (IgG), DA1E, Cell Signaling Technology] was used as a negative control. Signals from live cell fractions were used for analysis.

Quantification of protein localization in gel-encapsulated live cells

To visualize TNFR1 or F-actin, cells were first transfected with *TNFR1-YFP* or *mTagRFP-T-LifeAct-7* ("*LifeAct-RFP*"). A plasmid that contains *TNFR1-YFP* was a gift from J. A. Schmid (Addgene plasmid #111209). *mTagRFP-T-Lifeact-7* was a gift from M. Davidson (Addgene plasmid # 54586). Each plasmid (2 µg) and 500,000 cells were mixed in 100 µl of nucleofection buffer from the human MSC nucleofector kit (VPE-1001, Lonza) and electroporated using a high-viability program in Amaxa (Lonza). Transfected cells were then cultured overnight. After encapsulating cells in soft or stiff alginate-RGD gels, they were cultured for an additional day. Cells in 3D gels were then stained with 1 µM CellTrace Far Red (C34572, Thermo Fisher Scientific) for 1 hour in 37°C to label the cytoplasm. Prior to imaging, 1 µM ethidium bromide was added to exclude dead cells. 3D scanning of encapsulated cells expressing *TNFR1-YFP* and/or *LifeAct-RFP* was done on a Zeiss laser scanning microscope (LSM 710) with 40× objective. To quantify clustering of TNFR1 in response to TNFα, TNFα (100 ng/ml) was added to cells in 3D gels, and imaging was done after 20 min. BioImageXD, an open-source software, was used as described (*60*) to determine the outer boundary of the CellTrace Far Red signals by thresholding and Gaussian filtering so that TNFR1-YFP molecules localized on the boundary ("cell surface") versus those inside the cytoplasm could be distinguished. The built-in algorithms were then used after automatic thresholding (level 0.5) to quantify signal intensity, cluster size, and cluster number of TNFR1-YFP. To quantify both F-actin and TNFR1 near the cell surface, gel-encapsulated cells were preincubated with either dimethyl sulfoxide (DMSO) or nystatin (50 µM) for 2 hours, followed by TNFα stimulation for 20 min. Cells that express both TNFR1-YFP and LifeAct-RFP were then imaged, followed by analysis using Imaris 7.7 (Bitplane). Thresholding values were kept constant across all samples. Gaussian filtering was used to smooth the CellTrace signal, and the outer boundary of the reconstructed voxel was defined as the cell surface. A TNFR1 cluster was defined as any distinct TNFR1-YFP signal on the cell surface with voxel volume >0.1 μm^3. Analysis was done on every single TNFR1-YFP cluster for each cell. For each TNFR1-YFP cluster on the cell surface, a region of interest (2 µm by 1 µm by 1 µm) was drawn, and the corresponding LifeAct-RFP volume within the region was analyzed. As a control, LifeAct-RFP signals were also quantified near the cell surface regions where TNFR1-YFP clusters were not present.

Evaluation of TNFα binding to cells

After culturing gel-encapsulated cells for 1 day, DMSO or chemical inhibitors (latrunculin A, blebbistatin, or nystatin, purchased from Cayman Chemical) were added and incubated for 2 hours at 37°C. Cells were then rapidly retrieved on ice as described in characterization of NF-κB activation kinetics, but they were not fixed. Retrieved cells were incubated with biotinylated TNFα (R&D Systems) at saturating concentration (1 µg/ml) for 1 hour, followed by avidin–fluorescein isothiocyanate (FITC) for 30 min on ice. Flow cytometry analysis was then performed. The sample incubated with avidin-FITC alone was used as a negative control.

Coculture studies to evaluate effects of MSCs on hematopoiesis in vitro

Human cord blood $CD34^+$ cells from mixed donors were purchased from ZenBio (SER-CD34-F). Cord blood cells were first precultured in the StemSpan-II medium (#09605, STEMCELL Technology) supplemented with stem cell factor (SCF; 50 ng/ml), thrombopoietin (Tpo; 50 ng/ml), and 1% P/S for 8 days. In parallel, human MSCs were either plated on 2D plastic culture or encapsulated in 3D soft or stiff alginate-RGD gel for 1 day, followed by stimulation with or without TNFα (100 ng/ml) for 3 days. Precultured cord blood cells (5000) and 1677 primed MSCs (3:1 ratio) were then retrieved and cocultured in the 0.5% LF200 alginate-RGD fluid dissolved in the StemSpan-II medium supplemented with SCF (20 ng/ml), Tpo (20 ng/ml), and 1% P/S on the ultralow-binding 96-well plate (Sigma-Aldrich) for 4 days. Cells were then analyzed for human hematopoietic stem and progenitor cell subpopulations and monocyte lineages by flow cytometry after staining with the following antibodies based on previous studies (*33*, *34*): APC/Cy7 anti-human CD34 (581), phycoerythrin (PE)/Cy7 anti-human CD38 (HIT8a), APC anti-human CD90 (5E10), PE CD45RA (HI100), PE/Dazzle CD135 (BV10A4H2), FITC anti-human CD14 (HCD14), and Pacific Blue anti-human CD16 (3G8), all purchased from BioLegend.

Xenograft studies to evaluate effects of human MSCs on human monocyte production in vivo

All animal work was performed in compliance with the National Institutes of Health and institutional guidelines approved by the ethical committee from the University of Illinois at Chicago. Human cord blood $CD34^+$ cells (20,000) were injected retroorbitally into sublethally irradiated 8- to 12-week-old NOD/SCID/IL-$2\gamma^{-/-}$ (NSG) mice. After 2 weeks, all of the hair surrounding the knee joint was removed. MSCs from gels were retrieved by digesting them with alginate lyase in DMEM for 20 min at 37°C. Ex vivo conditioned human MSCs (10,000) were resuspended in 10 μl of PBS and delivered into the marrow cavity of the right tibia through the patellar tendon using an insulin syringe (28-gauge needle). PBS with no cell was delivered to the left tibia. After 4 days, mice were euthanized, the marrow from each tibia was flushed out, and cells were analyzed for human monocyte lineages by flow cytometry after staining with 7-AAD for cell viability and the following antibodies: APC anti-mouse CD45 (30-F11), PE-Cy7 anti-human CD45 (HI30), FITC anti-human CD14 (HCD14), and Pacific Blue anti-human CD16 (3G8), all purchased from BioLegend.

Tracking biodistribution of transplanted cells in vivo

After delivering firefly-expressing MSCs to NSG mice, their in vivo residence kinetics was evaluated. At different time points, 1.5 mg of D-luciferin in 200 μl of PBS was injected retroorbitally per 20 g of mouse followed by luminescence imaging with the IVIS Spectrum (PerkinElmer) within 10 min of injection. Average radiance (photons/s/cm^2/sr) from each time point was measured from each tibia.

Transwell migration assay

Transwell inserts with polycarbonate membrane with 3-μm pore size (Corning) were coated with fibronectin (10 μg/ml) in HBSS overnight at 4°C, followed by blocking with 1% BSA in HBSS for 1 hour at RT. The conditioned media were collected from gel-encapsulated human MSCs that are cultured in the presence or absence of TNFα (100 ng/ml) for 1 day, followed by washout and cultured in the absence of TNFα for another day. The same cell number per gel (~50,000 per 8-mm disc) was used to collect the conditioned media. Fresh human peripheral mononuclear cells (~100,000) were added to the top wells in serum-free FluoroBrite DMEM, while the conditioned media were added to the bottom wells. In some experiments, the conditioned media were incubated with the neutralizing antibody against human CCL2 (MAB679, R&D Systems) or the mouse IgG2B isotype control (MAB004, R&D Systems) for 3 hours at 4°C prior to the migration assay. The cells were allowed to migrate for 3 hours at 37°C, 5% CO_2. The cells collected from the bottom wells were subject to flow cytometry analysis for different lineages using the following anti-human antibodies: FITC CD14 (HCD14), APC CD4 (RPA-T4), APC-cy7 CD8 (SK1), PE CD19 (HIB19), and PE-cy7 CD56 (HCD56), all purchased from BioLegend. The cell number per sample was counted by adding a predefined number of polystyrene beads (Spherotech). The fraction of migrated cells was calculated by dividing with the total number of cells for each lineage added to each well.

Statistical analyses

All statistical analyses were performed using GraphPad Prism 6. Unless otherwise noted, all statistical comparisons were made from at least three independent experiments by one-way analysis of variance (ANOVA), followed by Tukey's post hoc testing, and were considered significant if $P < 0.05$.

SUPPLEMENTARY MATERIALS

Supplementary material for this article is available at http://advances.sciencemag.org/cgi/content/full/6/15/eaaw0158/DC1

View/request a protocol for this paper from *Bio-protocol*.

REFERENCES AND NOTES

1. R. Yue, B. O. Zhou, I. S. Shimada, Z. Zhao, S. J. Morrison, Leptin receptor promotes adipogenesis and reduces osteogenesis by regulating mesenchymal stromal cells in adult bone marrow. *Cell Stem Cell* **18**, 782–796 (2016).
2. S. Méndez-Ferrer, V. Michurina, F. Ferraro, A. R. Mazloom, B. D. Macarthur, S. A. Lira, D. T. Scadden, A. Ma'ayan, G. N. Enikolopov, P. S. Frenette, Mesenchymal and haematopoietic stem cells form a unique bone marrow niche. *Nature* **466**, 829–834 (2010).
3. A. Bartholomew, C. Sturgeon, M. Siatskas, K. Ferrer, K. McIntosh, S. Patil, W. Hardy, S. Devine, D. Ucker, R. Deans, A. Moseley, R. Hoffman, Mesenchymal stem cells suppress lymphocyte proliferation in vitro and prolong skin graft survival in vivo. *Exp. Hematol.* **30**, 42–48 (2002).
4. K. Le Blanc, D. Mougiakakos, Multipotent mesenchymal stromal cells and the innate immune system. *Nat. Rev. Immunol.* **12**, 383–396 (2012).
5. B. Parekkadan, J. M. Milwid, Mesenchymal stem cells as therapeutics. *Annu. Rev. Biomed. Eng.* **12**, 87–117 (2010).
6. Y. Wang, X. Chen, W. Cao, Y. Shi, Plasticity of mesenchymal stem cells in immunomodulation: Pathological and therapeutic implications. *Nat. Immunol.* **15**, 1009–1016 (2014).
7. C. Shi, T. Jia, S. Mendez-Ferrer, T. M. Hohl, N. V. Serbina, L. Lipuma, I. Leiner, M. O. Li, P. S. Frenette, E. G. Pamer, Bone marrow mesenchymal stem and progenitor cells induce monocyte emigration in response to circulating toll-like receptor ligands. *Immunity* **34**, 590–601 (2011).
8. K. Németh, A. Leelahavanichkul, P. S. Yuen, B. Mayer, A. Parmelee, K. Doi, P. G. Robey, K. Leelahavanichkul, B. H. Koller, J. M. Brown, X. Hu, I. Jelinek, R. A. Star, E. Mezey, Bone marrow stromal cells attenuate sepsis via prostaglandin E(2)-dependent reprogramming of host macrophages to increase their interleukin-10 production. *Nat. Med.* **15**, 42–49 (2009).
9. R. H. Lee, A. A. Pulin, M. J. Seo, D. J. Kota, J. Ylostalo, B. L. Larson, L. Semprun-Prieto, P. Delafontaine, D. J. Prockop, Intravenous hMSCs improve myocardial infarction in mice because cells embolized in lung are activated to secrete the anti-inflammatory protein TSG-6. *Cell Stem Cell* **5**, 54–63 (2009).
10. D. M. Mosser, J. P. Edwards, Exploring the full spectrum of macrophage activation. *Nat. Rev. Immunol.* **8**, 958–969 (2008).

11. L. Ding, T. L. Saunders, G. Enikolopov, S. J. Morrison, Endothelial and perivascular cells maintain haematopoietic stem cells. *Nature* **481**, 457–462 (2012).
12. D. Park, J. A. Spencer, B. I. Koh, T. Kobayashi, J. Fujisaki, T. L. Clemens, C. P. Lin, H. M. Kronenberg, D. T. Scadden, Endogenous bone marrow MSCs are dynamic, fate-restricted participants in bone maintenance and regeneration. *Cell Stem Cell* **10**, 259–272 (2012).
13. I. L. Ivanovska, J. Swift, K. Spinler, D. Dingal, S. Cho, D. E. Discher, Cross-linked matrix rigidity and soluble retinoids synergize in nuclear lamina regulation of stem cell differentiation. *Mol. Biol. Cell* **28**, 2010–2022 (2017).
14. Z. Zhong, O. Akkus, Effects of age and shear rate on the rheological properties of human yellow bone marrow. *Biorheology* **48**, 89–97 (2011).
15. A. J. Engler, S. Sen, H. L. Sweeney, D. E. Discher, Matrix elasticity directs stem cell lineage specification. *Cell* **126**, 677–689 (2006).
16. O. Chaudhuri, L. Gu, D. Klumpers, M. Darnell, S. A. Bencherif, J. C. Weaver, N. Huebsch, H. P. Lee, E. Lippens, G. N. Duda, D. J. Mooney, Hydrogels with tunable stress relaxation regulate stem cell fate and activity. *Nat. Mater.* **15**, 326–334 (2016).
17. A. A. Abdeen, J. B. Weiss, J. Lee, K. A. Kilian, Matrix composition and mechanics direct proangiogenic signaling from mesenchymal stem cells. *Tissue Eng. Part A* **20**, 2737–2745 (2014).
18. F. D. Liu, N. Pishesha, Z. Poon, T. Kaushik, K. J. Van Vliet, Material viscoelastic properties modulate the mesenchymal stem cell secretome for applications in hematopoietic recovery. *ACS Biomater Sci. Eng.* **3**, 3292–3306 (2017).
19. G. Valles, F. Bensiamar, L. Crespo, M. Arruebo, N. Vilaboa, L. Saldaña, Topographical cues regulate the crosstalk between MSCs and macrophages. *Biomaterials* **37**, 124–133 (2015).
20. F. D. Liu, K. Tam, N. Pishesha, Z. Poon, K. J. Van Vliet, Improving hematopoietic recovery through modeling and modulation of the mesenchymal stromal cell secretome. *Stem Cell Res. Ther.* **9**, 268 (2018).
21. X. Huang, B. Zhu, X. Wang, R. Xiao, C. Wang, Three-dimensional co-culture of mesenchymal stromal cells and differentiated osteoblasts on human bio-derived bone scaffolds supports active multi-lineage hematopoiesis in vitro: Functional implication of the biomimetic HSC niche. *Int. J. Mol. Med.* **38**, 1141–1151 (2016).
22. G. Ren, X. Zhao, Y. Wang, X. Zhang, X. Chen, C. Xu, Z. R. Yuan, A. I. Roberts, L. Zhang, B. Zheng, T. Wen, Y. Han, A. B. Rabson, J. A. Tischfield, C. Shao, Y. Shi, CCR2-dependent recruitment of macrophages by tumor-educated mesenchymal stromal cells promotes tumor development and is mimicked by TNFα. *Cell Stem Cell* **11**, 812–824 (2012).
23. K. Nakamura, T. Kouro, P. W. Kincade, A. Malykhin, K. Maeda, K. M. Coggeshall, Src homology 2-containing 5-inositol phosphatase (SHIP) suppresses an early stage of lymphoid cell development through elevated interleukin-6 production by myeloid cells in bone marrow. *J. Exp. Med.* **199**, 243–254 (2004).
24. A. Hoffmann, A. Levchenko, M. L. Scott, D. Baltimore, The IkappaB-NF-kappaB signaling module: Temporal control and selective gene activation. *Science* **298**, 1241–1245 (2002).
25. S. Mangan, S. Itzkovitz, A. Zaslaver, U. Alon, The incoherent feed-forward loop accelerates the response-time of the gal system of Escherichia coli. *J. Mol. Biol.* **356**, 1073–1081 (2006).
26. D. V. Bax, A. J. Messent, J. Tart, M. van Hoang, J. Kott, R. A. Maciewicz, M. J. Humphries, Integrin alpha5beta1 and ADAM-17 interact in vitro and co-localize in migrating HeLa cells. *J. Biol. Chem.* **279**, 22377–22386 (2004).
27. P. E. Morton, C. Perrin, J. Levitt, D. R. Matthews, R. J. Marsh, R. Pike, D. McMillan, A. Maloney, S. Poland, S. Ameer-Beg, M. Parsons, TNFR1 membrane reorganization promotes distinct modes of TNFα signaling. *Sci. Signal.* **12**, eaaw2418 (2019).
28. M. Foti, G. Porcheron, M. Fournier, C. Maeder, J. L. Carpentier, The neck of caveolae is a distinct plasma membrane subdomain that concentrates insulin receptors in 3T3-L1 adipocytes. *Proc. Natl. Acad. Sci. U.S.A.* **104**, 1242–1247 (2007).
29. D. F. Legler, O. Micheau, M. A. Doucey, J. Tschopp, C. Bron, Recruitment of TNF receptor 1 to lipid rafts is essential for TNFα-Mediated NF-κB activation. *Immunity* **18**, 655–664 (2003).
30. B. Sinha, D. Köster, R. Ruez, P. Gonnord, M. Bastiani, D. Abankwa, R. V. Stan, G. Butler-Browne, B. Vedie, L. Johannes, N. Morone, R. G. Parton, G. Raposo, P. Sens, C. Lamaze, P. Nassoy, Cells respond to mechanical stress by rapid disassembly of caveolae. *Cell* **144**, 402–413 (2011).
31. J. Riedl, A. H. Crevenna, K. Kessenbrock, J. H. Yu, D. Neukirchen, M. Bista, F. Bradke, D. Jenne, T. A. Holak, Z. Werb, M. Sixt, R. Wedlich-Soldner, Lifeact: A versatile marker to visualize F-actin. *Nat. Methods* **5**, 605–607 (2008).
32. J. W. Shin, D. J. Mooney, Extracellular matrix stiffness causes systematic variations in proliferation and chemosensitivity in myeloid leukemias. *Proc. Natl. Acad. Sci. U.S.A.* **113**, 12126–12131 (2016).
33. M. G. Manz, T. Miyamoto, K. Akashi, I. L. Weissman, Prospective isolation of human clonogenic common myeloid progenitors. *Proc. Natl. Acad. Sci. U.S.A.* **99**, 11872–11877 (2002).
34. R. Majeti, C. Y. Park, I. L. Weissman, Identification of a hierarchy of multipotent hematopoietic progenitors in human cord blood. *Cell Stem Cell* **1**, 635–645 (2007).
35. H. Glimm, W. Eisterer, K. Lee, J. Cashman, T. L. Holyoake, F. Nicolini, L. D. Shultz, C. von Kalle, C. J. Eaves, Previously undetected human hematopoietic cell populations with short-term repopulating activity selectively engraft NOD/SCID-β2 microglobulin-null mice. *J. Clin. Invest.* **107**, 199–206 (2001).
36. A. A. Patel, Y. Zhang, J. N. Fullerton, L. Boelen, A. Rongvaux, A. A. Maini, V. Bigley, R. A. Flavell, D. W. Gilroy, B. Asquith, D. Macallan, S. Yona, The fate and lifespan of human monocyte subsets in steady state and systemic inflammation. *J. Exp. Med.* **214**, 1913–1923 (2017).
37. A. Rongvaux, T. Willinger, J. Martinek, T. Strowig, S. V. Gearty, L. L. Teichmann, Y. Saito, F. Marches, S. Halene, A. K. Palucka, M. G. Manz, R. A. Flavell, Development and function of human innate immune cells in a humanized mouse model. *Nat. Biotechnol.* **32**, 364–372 (2014).
38. D. Schauer, P. Starlinger, P. Zajc, L. Alidzanovic, T. Maier, E. Buchberger, L. Pop, B. Gruenberger, T. Gruenberger, C. Brostjan, Monocytes with angiogenic potential are selectively induced by liver resection and accumulate near the site of liver regeneration. *BMC Immunol.* **15**, 50 (2014).
39. S. I. Grivennikov, A. V. Tumanov, D. J. Liepinsh, A. A. Kruglov, B. I. Marakusha, A. N. Shakhov, T. Murakami, L. N. Drutskaya, I. Förster, B. E. Clausen, L. Tessarollo, B. Ryffel, D. V. Kuprash, S. A. Nedospasov, Distinct and nonredundant in vivo functions of TNF produced by t cells and macrophages/neutrophils: Protective and deleterious effects. *Immunity* **22**, 93–104 (2005).
40. Y. Wolf, A. Shemer, M. Polonsky, M. Gross, A. Mildner, S. Yona, E. David, K. W. Kim, T. Goldmann, I. Amit, M. Heikenwalder, S. Nedospasov, M. Prinz, N. Friedman, S. Jung, Autonomous TNF is critical for in vivo monocyte survival in steady state and inflammation. *J. Exp. Med.* **214**, 905–917 (2017).
41. R. E. Lee, S. R. Walker, K. Savery, D. A. Frank, S. Gaudet, Fold change of nuclear NF-κB determines TNF-induced transcription in single cells. *Mol. Cell* **53**, 867–879 (2014).
42. J. Chew, S. Biswas, S. Shreeram, M. Humaidi, E. T. Wong, M. K. Dhillion, H. Teo, A. Hazra, C. C. Fang, E. López-Collazo, D. V. Bulavin, V. Tergaonkar, WIP1 phosphatase is a negative regulator of NF-kappaB signalling. *Nat. Cell Biol.* **11**, 659–666 (2009).
43. M. Brechmann, T. Mock, D. Nickles, M. Kiessling, N. Weit, R. Breuer, W. Müller, G. Wabnitz, F. Frey, J. P. Nicolay, N. Booken, Y. Samstag, C. D. Klemke, M. Herling, M. Boutros, P. H. Krammer, R. Arnold, A PP4 holoenzyme balances physiological and oncogenic nuclear factor-kappa B signaling in T lymphocytes. *Immunity* **37**, 697–708 (2012).
44. M. K. Brunialti, E. G. Kallas, M. Freudenberg, C. Galanos, R. Salomao, Influence of EDTA and heparin on lipopolysaccharide binding and cell activation, evaluated at single-cell level in whole blood. *Cytometry* **50**, 14–18 (2002).
45. J. Du, X. Chen, X. Liang, G. Zhang, J. Xu, L. He, Q. Zhan, X. Q. Feng, S. Chien, C. Yang, Integrin activation and internalization on soft ECM as a mechanism of induction of stem cell differentiation by ECM elasticity. *Proc. Natl. Acad. Sci. U.S.A.* **108**, 9466–9471 (2011).
46. C. H. Yu, N. B. M. Rafiq, F. Cao, Y. Zhou, A. Krishnasamy, K. H. Biswas, A. Ravasio, Z. Chen, Y. H. Wang, K. Kawauchi, G. E. Jones, M. P. Sheetz, Integrin-beta3 clusters recruit clathrin-mediated endocytic machinery in the absence of traction force. *Nat. Commun.* **6**, 8672 (2015).
47. A. Mitra, S. Venkatachalapathy, P. Ratna, Y. Wang, D. S. Jokhun, G. V. Shivashankar, Cell geometry dictates TNFα-induced genome response. *Proc. Natl. Acad. Sci. U.S.A.* **114**, E3882–E3891 (2017).
48. N. Huebsch, P. R. Arany, A. S. Mao, D. Shvartsman, O. A. Ali, S. A. Bencherif, J. Rivera-Feliciano, D. J. Mooney, Harnessing traction-mediated manipulation of the cell/matrix interface to control stem-cell fate. *Nat. Mater.* **9**, 518–526 (2010).
49. G. Sabio, R. J. Davis, TNF and MAP kinase signalling pathways. *Semin. Immunol.* **26**, 237–245 (2014).
50. Y. Deng, X. Ren, L. Yang, Y. Lin, X. Wu, A JNK-dependent pathway is required for TNFalpha-induced apoptosis. *Cell* **115**, 61–70 (2003).
51. C. J. Pronk, O. P. Veiby, D. Bryder, S. E. Jacobsen, Tumor necrosis factor restricts hematopoietic stem cell activity in mice: Involvement of two distinct receptors. *J. Exp. Med.* **208**, 1563–1570 (2011).
52. A. M. Bailey, M. Mendicino, P. Au, An FDA perspective on preclinical development of cell-based regenerative medicine products. *Nat. Biotechnol.* **32**, 721–723 (2014).
53. J. W. Shin, K. R. Spinler, J. Swift, J. A. Chasis, N. Mohandas, D. E. Discher, Lamins regulate cell trafficking and lineage maturation of adult human hematopoietic cells. *Proc. Natl. Acad. Sci. U.S.A.* **110**, 18892–18897 (2013).
54. T. Harada, J. Swift, J. Irianto, J. W. Shin, K. R. Spinler, A. Athirasala, R. Diegmiller, P. C. D. P. Dingal, I. L. Ivanovska, D. E. Discher, Nuclear lamin stiffness is a barrier to 3D migration, but softness can limit survival. *J. Cell Biol.* **204**, 669–682 (2014).
55. Y. Muguruma, T. Yahata, H. Miyatake, T. Sato, T. Uno, J. Itoh, S. Kato, M. Ito, T. Hotta, K. Ando, Reconstitution of the functional human hematopoietic microenvironment derived from human mesenchymal stem cells in the murine bone marrow compartment. *Blood* **107**, 1878–1887 (2006).
56. S. F. H. de Witte, F. Luk, J. M. Sierra Parraga, M. Gargesha, A. Merino, S. S. Korevaar, A. S. Shankar, L. O'Flynn, S. J. Elliman, D. Roy, M. G. H. Betjes, P. N. Newsome, C. C. Baan, M. J. Hoogduijn, Immunomodulation by therapeutic Mesenchymal Stromal Cells (MSC) is

triggered through phagocytosis of MSC By monocytic cells. *Stem Cells* **36**, 602–615 (2018).
57. T. Y. Wong, L. A. Preston, N. L. Schiller, Alginate lyase: Review of major sources and enzyme characteristics, structure-function analysis, biological roles, and applications. *Annu. Rev. Microbiol.* **54**, 289–340 (2000).
58. M. P. Lutolf, J. L. Lauer-Fields, H. G. Schmoekel, A. T. Metters, F. E. Weber, G. B. Fields, J. A. Hubbell, Synthetic matrix metalloproteinase-sensitive hydrogels for the conduction of tissue regeneration: Engineering cell-invasion characteristics. *Proc. Natl. Acad. Sci. U.S.A.* **100**, 5413–5418 (2003).
59. A. S. Mao, J. W. Shin, S. Utech, H. Wang, O. Uzun, W. Li, M. Cooper, Y. Hu, L. Zhang, D. A. Weitz, D. J. Mooney, Deterministic encapsulation of single cells in thin tunable microgels for niche modelling and therapeutic delivery. *Nat. Mater.* **16**, 236–243 (2017).
60. P. Kankaanpää, L. Paavolainen, S. Tiitta, M. Karjalainen, J. Päivärinne, J. Nieminen, V. Marjomäki, J. Heino, D. J. White, BioImageXD: An open, general-purpose and high-throughput image-processing platform. *Nat. Methods* **9**, 683–689 (2012).

Acknowledgments: We gratefully acknowledge the Research Open Access Publishing (ROAAP) Fund of the University of Illinois at Chicago for financial support towards the open access publishing fee for this article. The atomic force microscopy work was performed in part at the Center for Nanoscale Systems (CNS), a member of the National Nanotechnology Coordinated Infrastructure Network (NNCI), which is supported by the National Science Foundation under NSF award no. 1541959. CNS is part of Harvard University. **Funding:** This work was supported by NIH grant R01HL141255 (J.-W.S.), R00HL125884 (J.-W.S.), and R01EB023287 (D.J.M.). **Author contributions:** S.W.W., S.L., M.H.C., D.J.M., and J.-W.S. designed the research. S.W.W., S.L., M.H.C., and J.-W.S. performed the research. S.W.W., S.L., D.J.M., and J.-W.S. wrote the paper. **Competing interests:** All authors declare that they have no competing interests. **Data and materials availability:** All data needed to evaluate the conclusions in the paper are present in the paper and/or the Supplementary Materials. Additional data related to this paper may be requested from the authors.

Submitted 12 November 2018
Accepted 14 January 2020
Published 8 April 2020
10.1126/sciadv.aaw0158

Citation: S. W. Wong, S. Lenzini, M. H. Cooper, D. J. Mooney, J.-W. Shin, Soft extracellular matrix enhances inflammatory activation of mesenchymal stromal cells to induce monocyte production and trafficking. *Sci. Adv.* **6**, eaaw0158 (2020).

ScienceAdvances

Soft extracellular matrix enhances inflammatory activation of mesenchymal stromal cells to induce monocyte production and trafficking

Sing Wan Wong, Stephen Lenzini, Madeline H. Cooper, David J. Mooney and Jae-Won Shin

Sci Adv **6** (15), eaaw0158.
DOI: 10.1126/sciadv.aaw0158

Science Advances (ISSN 2375-2548) is published by the American Association for the Advancement of Science, 1200 New York Avenue NW, Washington, DC 20005. The title *Science Advances* is a registered trademark of AAAS.

Science Advances
AAAS

advances.sciencemag.org/cgi/content/full/6/15/eaaw0158/DC1

Supplementary Materials for

Soft extracellular matrix enhances inflammatory activation of mesenchymal stromal cells to induce monocyte production and trafficking

Sing Wan Wong, Stephen Lenzini, Madeline H. Cooper, David J. Mooney*, Jae-Won Shin*

*Corresponding author. Email: mooneyd@seas.harvard.edu (D.J.M.); shinjw@uic.edu (J.-W.S.)

Published 8 April 2020, *Sci. Adv.* **6**, eaaw0158 (2020)
DOI: 10.1126/sciadv.aaw0158

This PDF file includes:

Mathematical modeling

TNFα-mediated NF-κB activation

The fraction of an interacting protein X bound to a target Y is generally described by a standard Hill function:

$$\theta_X^Y = \frac{1}{1 + \left(\frac{K_X^Y}{[X]}\right)^n} \qquad (Eq. 1.1).$$

K_X^Y is the concentration of X where the total bound protein complex is half-maximum (***potency***). n denotes cooperativity of binding, which is typically 1 or 2 (*25*).

θ_X^Y is used to describe stimulation upon binding, while $1 - \theta_X^Y$ is used to describe repression.

We constructed a set of differential equations to describe the kinetics of NF-κB activation (phosphorylated p65) in response to TNFα binding to TNF receptor (TNFR). We implemented an incoherent feedforward loop (I1-FFL) where TNFR stimulation leads to NF-κB activation and induction of factors that in turn inhibit activated NF-κB (**Fig. S2C**).

$$\frac{dI}{dt} = \beta_I \theta_{TNF\alpha}^{TNFR} - \alpha_I I \qquad (Eq. 1.2)$$

where *I* is the concentration of factors that are induced upon TNFR stimulation, which subsequently inhibit activated NF-κB (deemed 'inhibitors'). β_I is the intrinsic or constitutive production rate of *I*. $\theta_{TNF\alpha}^{TNFR}$ denotes dose response for stimulation of TNFR by TNFα (*Eq*. 1.1). α_I is the decay rate of *I*.

$$\frac{dpNF}{dt} = \beta_{pNF} \theta_{TNF\alpha}^{TNFR} (1 - \theta_I^{pNF}) - \alpha_{pNF} pNF \qquad (Eq. 1.3)$$

,where *pNF* is the concentration of activated NF-κB. β_{pNF} is the intrinsic or constitutive production rate of *pNF*. $1 - \theta_I^{pNF}$ denotes dose response for repression of *pNF* by *I*. Both

stimulated TNFR and *I* determine *pNF*, and hence their functions are multiplied (*25*). α_{pNF} is the decay rate of *pNF*.

Analytical solution of $Eq.$ 1.3 leads to:

$$pNF = \frac{\beta_{pNF}}{\alpha_{pNF}}\theta_{TNF\alpha}^{TNFR}(1-\theta_I^{pNF}) + Ce^{-\alpha_{pNF}t} \qquad (Eq.1.4)$$

At t = 0,

$$pNF_0 = \frac{\beta_{pNF}}{\alpha_{pNF}}\theta_{TNF\alpha}^{TNFR}(1-\theta_I^{pNF}) + C \qquad (Eq.1.5)$$

Substituting Eq. 1.5 into Eq. 1.4, followed by rearrangement leads to:

$$pNF = \frac{\beta_{pNF}}{\alpha_{pNF}}\theta_{TNF\alpha}^{TNFR}(1-\theta_I^{pNF})(1-e^{-\alpha_{pNF}t}) + pNF_0e^{-\alpha_{pNF}t} \qquad (Eq.1.6)$$

The maximum level of *pNF* (pNF_m) occurs when the inhibition is 0, i.e. $(1-\theta_I^{pNF}) = 1$, and t = ∞. Thus,

$$pNF_m = \frac{\beta_{pNF}}{\alpha_{pNF}}\theta_{TNF\alpha}^{TNFR} \quad (Eq.1.7).$$

The equation for the fold change in *pNF* is:

$$F_{pNF} = \frac{pNF}{pNF_0} = F_{pNF_m}(1-\theta_I^{pNF})(1-e^{-\alpha_{pNF}t}) + e^{-\alpha_{pNF}t} \qquad (Eq.1.8)$$

where $F_{pNF_m} = \frac{pNF_m}{pNF_0}$.

Assuming that the initial level of *I* is very low (~0) (*42*, *43*), solving Eq. 1.2 leads to:

$$I = I_{st}\,(1 - e^{-\alpha_I t}) \quad (Eq.\,1.9)$$

where $I_{st} = \frac{\beta_I}{\alpha_I}\theta_{TNF\alpha}^{TNFR}$.

Substituting Eq. 1.9. into Eq 1.8., leads to:

$$F_{pNF} = F_{pNF_m}(1 - \frac{1}{1 + \left(\frac{K_I^{pNF}}{I_{st}(1-e^{\alpha_I t})}\right)^n})(1 - e^{-\alpha_{pNF} t}) + e^{-\alpha_{pNF} t} \quad (Eq.\,1.10)$$

In a simple case when n = 1, rearranging Eq. 1.10 leads to:

$$F_{pNF} = F_{pNF_m}(\frac{I_{ratio}}{I_{ratio} + (1 - e^{\alpha_I t})})(1 - e^{-\alpha_{pNF} t}) + e^{-\alpha_{pNF} t} \quad (Eq.\,1.11)$$

, where $I_{ratio} = \frac{K_I^{pNF}}{I_{st}}$

At the steady state ($F_{pNF_{st}}$), t = ∞,

$$F_{pNF_{st}} = F_{pNF_m}\left(\frac{I_{ratio}}{I_{ratio} + 1}\right) \quad (Eq.\,1.12)$$

The maximum to steady state ratio of *pNF* (R) = $\frac{F_{pNF_m}}{F_{pNF_{st}}} = \frac{pNF_m}{pNF_{st}}$ is constant because:

$\frac{soft\ pNF_m}{stiff\ pNF_m} = \frac{soft\ pNF_{st}}{stiff\ pNF_{st}}$ = ~1.6 when t ≥ 10 min after TNFα stimulation (**Fig. S2B**),

$$I_{ratio} = \left(\frac{1}{R - 1}\right) \quad (Eq.\,1.13).$$

Finally, substituting Eq. 1.13 to Eq. 1.11, and rearrangement leads to:

$$F_{pNF} = F_{pNF_m} \frac{1 - e^{-\alpha_{pNF}t}}{1 + (1 - e^{\alpha_I t})(R - 1)} + e^{-\alpha_{pNF}t} \qquad (Eq. 1.14)$$

; Hence, β_I no longer exists in this equation. pNF_0 is similar between soft and stiff substrates, which was experimentally determined. If pNF_0 is set to 1, *pNF* can be expressed simply as the fold change from the baseline (1.0). Thus,

$$pNF = pNF_m \frac{1 - e^{-\alpha_{pNF}t}}{1 + (1 - e^{\alpha_I t})(R - 1)} + e^{-\alpha_{pNF}t} \quad (Eq. 1.15).$$

Therefore, *I* affects *pNF* only via α_I.

R, pNF_m, α_I, and α_{pNF} were determined by fitting the experimental data to Eq. 1.15. Out of these parameters, fitting the data in **Fig. 2A** shows that only pNF_m (and thus pNF_{st}) is significantly different between soft and stiff substrates (**Fig. S2D**).

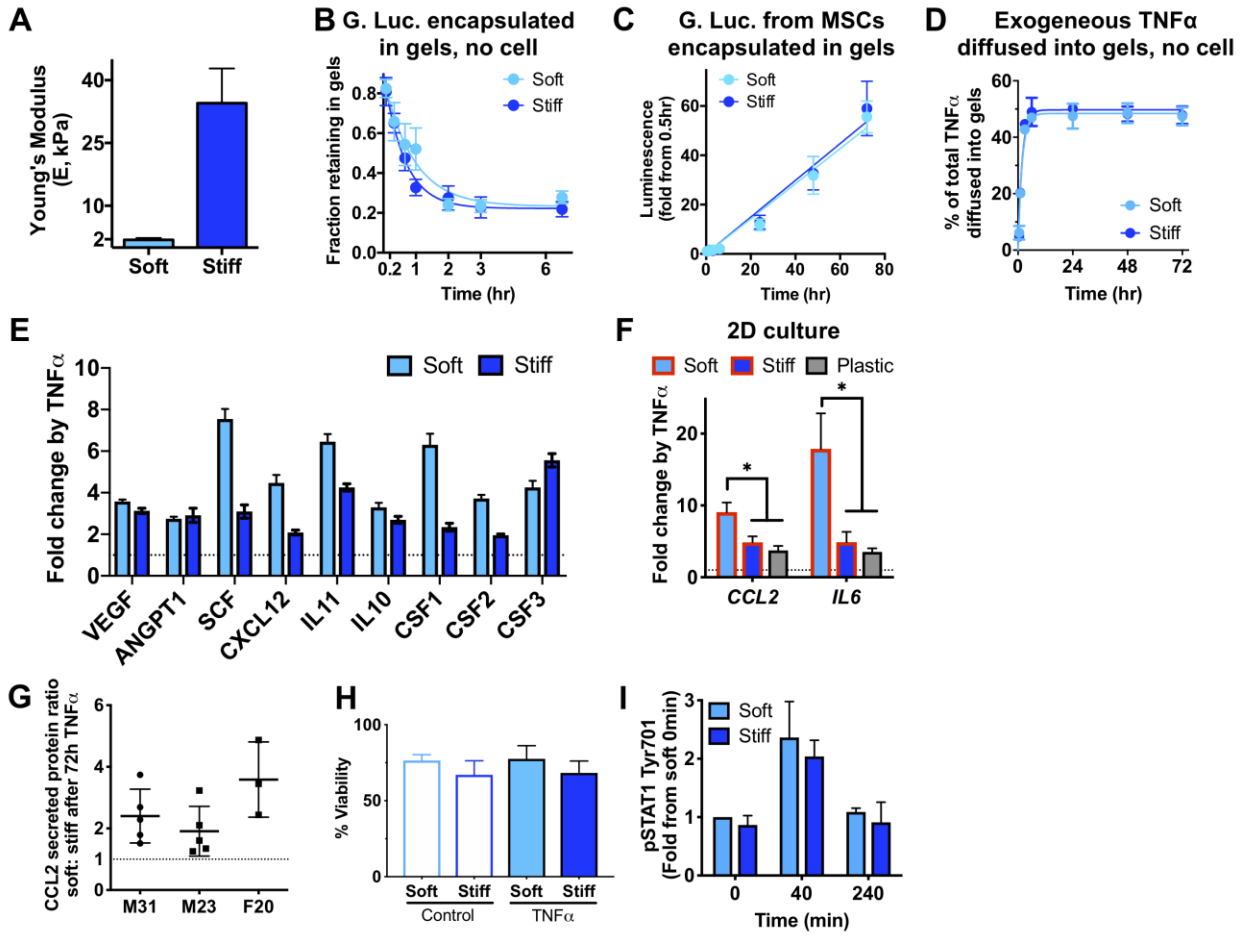

Figure S1. Characterization of soluble factor diffusion and response of MSCs to TNFα in engineered alginate hydrogels. **(A)** AFM was used to measure Young's modulus (*E*) of 'soft or 'stiff' alginate gels. Alginate hydrogels were formed by different calcium sulfate concentrations: 12~12.5 mM for soft (*E* ~2 kPa) and 35~40 mM for stiff (*E* ~ 35 kPa). Representative graphs from a batch of alginate-RGD. n ≥ 20 measurements. Error bars: ± SD. **(B)** Diffusion of *Gaussia luciferase* from ionic alginate hydrogels to media over time. The conditioned media from MSCs expressing *Gaussia luciferase* was mixed with alginate solutions to form soft or stiff gels, which were then punched into discs, followed by incubation in DMEM for 37°C. The gels were washed and digested into solutions by adding 50 mM EDTA at the indicated time points. The amount of *Gaussia luciferase* remaining in gels was normalized by that of total *Gaussia luciferase* encapsulated in gels. Half-time of protein diffusion = ~32 min for both soft and stiff gels. n = 3 technical replicates ± SD **(C)** Secretion kinetics of *Gaussia luciferase* from engineered MSCs in 3D alginate-RGD hydrogels. The media were collected at the indicated time points to measure the level of *Gaussia luciferase*. All the values were normalized by the signal at 30 min in culture.

Linear fit for both soft and stiff groups, slope = 0.7/hr. n = 3 experiments ± SEM. **(D)** Diffusion of exogenously added TNFα into soft or stiff alginate hydrogels. 100 ng/ml recombinant TNFα was added to soft or stiff gels and the amount of TNFα in gels at different time points was quantified by ELISA and normalized to total amount of TNFα added. One-phase association kinetics fit, $t_{1/2}$ = ~1.2hr, plateau = ~50% for both soft and stiff gels. n = 3 technical replicates ± SD. **(E)** Changes in mRNA expression of a panel of genes in response to treatment of TNFα for 3 days in soft or stiff gels. n = 3 technical replicates for each gene ± SD. **(F)** TNFα-induced upregulation of *CCL2* and *IL6* mRNAs in MSCs plated on 2D culture environments. For each gene, $P<0.05$ from one-way ANOVA with Tukey's HSD test, $^*P<0.05$ (n = 3 experiments). Error bars indicate ± SEM. **(G)** Fold difference in TNFα-induced CCL2 protein expression between MSCs in soft and stiff matrices across different donors. M/F: male or female; Number = age. Each data point is from an independent experiment (3~5 experiments per donor). **(H)** Percentage of viable (calcein positive, ethidium bromide negative) MSCs after encapsulation in soft or stiff 3D gels and culturing for 1 day. n = 3 experiments ± SEM. **(I)** Phosphorylation levels of STAT1 at Tyr701 in response to IFNγ in hydrogel-encapsulated MSCs evaluated by intracellular flow cytometry. n = 3 technical replicates ± SD.

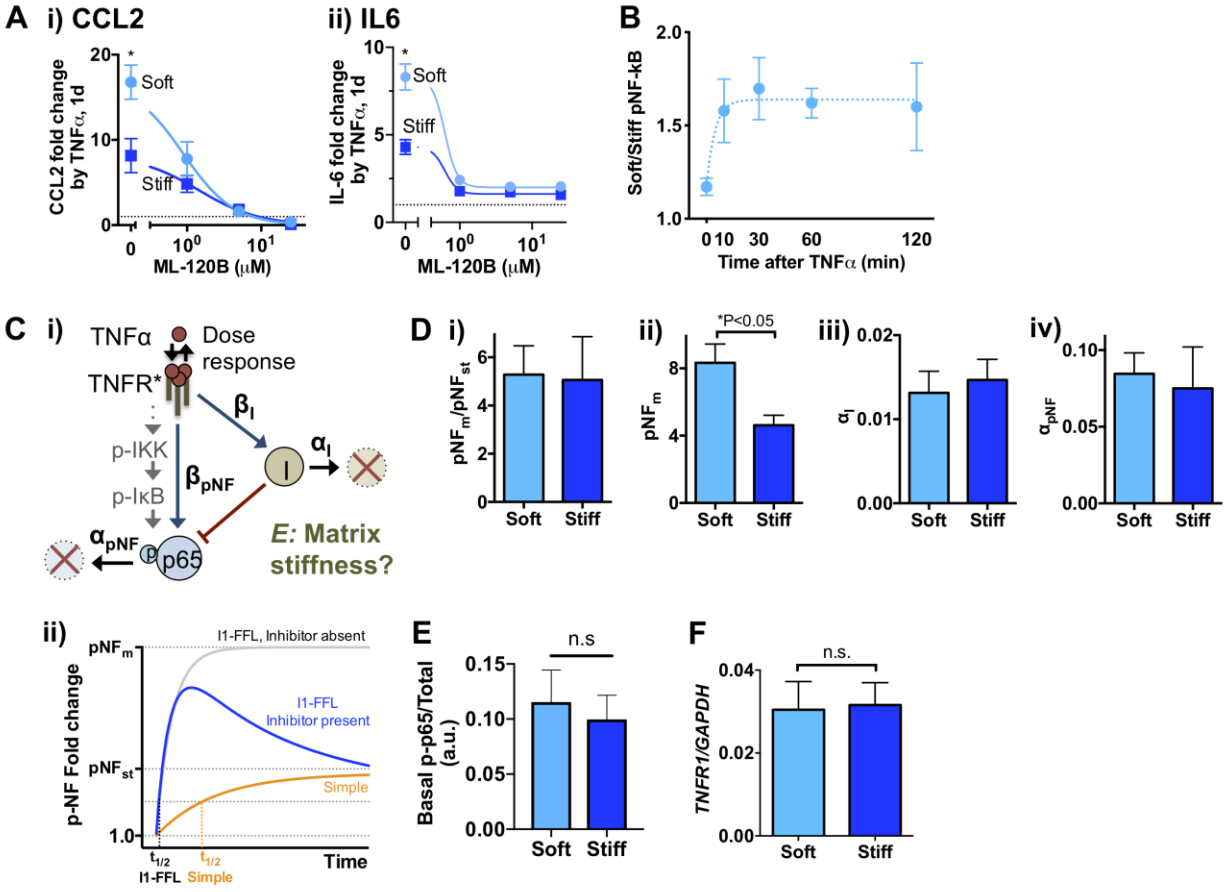

Figure S2. Characterization of TNFα-induced NF-κB activation kinetics and surface TNFR1 clustering in MSCs encapsulated in alginate-RGD hydrogels. **(A)** Upregulation of CCL2 and IL6 by TNFα requires IKK. Dose-response curves are shown in response to the IKK2 selective inhibitor ML-120B for 1 day. (i) CCL2, soft IC50 ~ 0.9 μM and stiff IC50 ~ 1.4 μM with Hill coefficient ~1.0 for both soft and stiff. (ii) IL6, IC50 ~ 0.6 μM with Hill coefficient ~1.5 for both soft and stiff. Paired T-test, *P<0.05 soft *vs*. stiff at each dose. n = 3 experiments ± SEM. **(B)** Experimental results showing the ratio of activated NF-κB in MSCs between soft and stiff substrates at different time points. One phase association kinetics fit shows plateau = ~1.6 at t ≥ 10 min. n = 3 experiments ± SEM. **(C)** (i) A modeling scheme showing a pulse generator circuit. β_I, intrinsic rate of inhibitor activation; α_I, decay rate of inhibitors; β_{pNF}**,** intrinsic rate of p65 activation (combined steps including IKK activation (p-IKK) and IκB degradation (p-IκB)); α_{pNF}**,** decay rate of activated p65. These components form an incoherent feedforward loop (I1-FFL). (ii) A representative graph of the I1-FFL model. In the absence of the inhibitor, activated

NF-κB reaches the maximum level (pNF_m). In the presence of the inhibitor, the I1-FFL model shows a pulse-like behavior where activation of NF-κB occurs rapidly followed by gradual deactivation, finally reaching the steady state (pNF_{st}). Compared to the simple regulation with the equivalent pNF_{st}, I1-FFL accelerates the response time ($t_{1/2}$). **(D)** Results from fitting the experimental data (**Fig. 2A**) to the I1-FFL based model. (i) pNF_m/pNF_{st}. (ii) pNF_m. (iii) The decay rate of the inhibitor (α_I). (iv) The decay rate of the activated NF-κB (α_{pNF}). n = 3 experiments ± SEM. **(E)** The basal level of phosphorylated NF-κB at Ser536 (p-p65) normalized to total p65. n = 3 experiments ± SEM. **(F)** Gene expression of *TNFR1* relative to *GAPDH* measured by qPCR. n = 3 technical replicates ± SD.

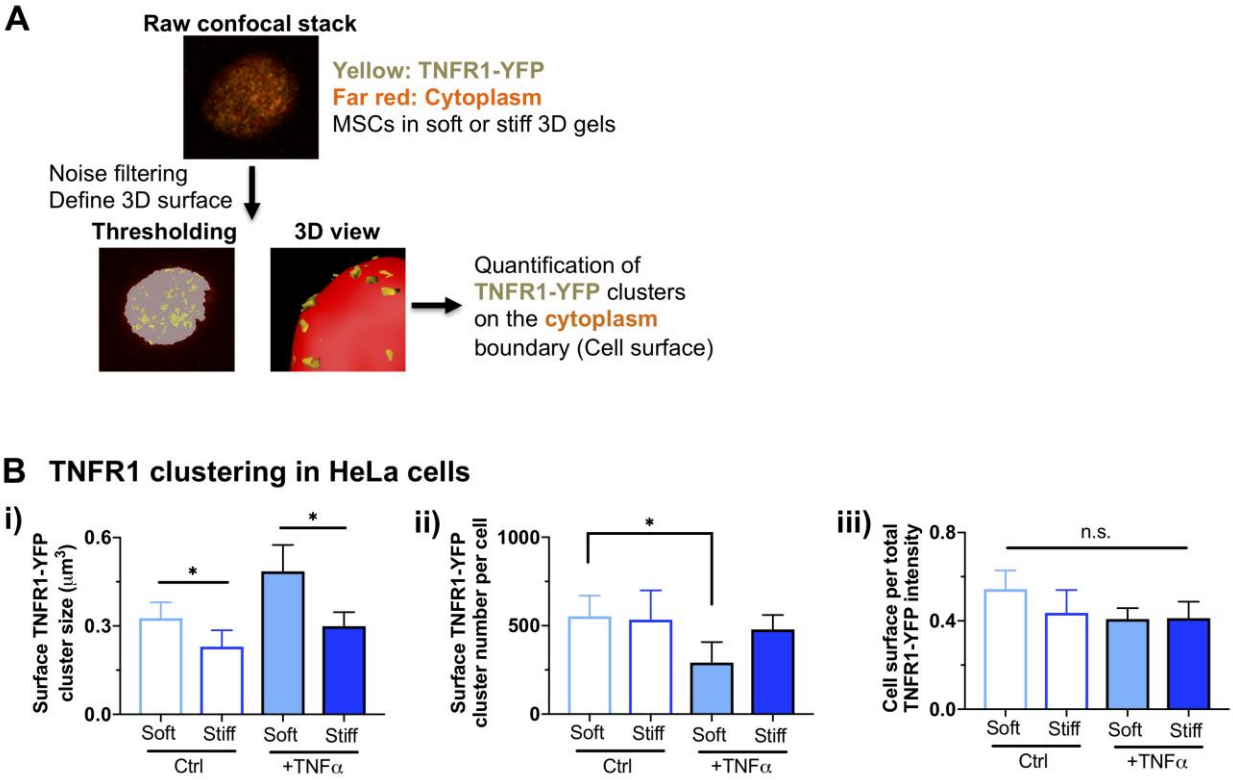

Figure S3. Characterization of TNFR1 clustering as a function of matrix stiffness. (A) An overview of the method to quantify cell surface clusters of TNFR1-YFP by using confocal imaging and image processing (see **Methods**). **(B)** Cell surface distribution and clustering of TNFR1-YFP in HeLa cells encapsulated in soft or stiff 3D gels. (i) Cluster size of TNFR1-YFP on the cell surface. (ii) Cluster number of TNFR1-YFP per cell. (iii) Cell surface per total TNFR1-YFP intensity. $P<0.05$ One-way Brown-Forsythe and Welch ANOVA for i and ii with Dunnett T3 multiple comparisons test, $^*P<0.05$ (n = 15 cells from 2 experiments). Error bars: ± SD.

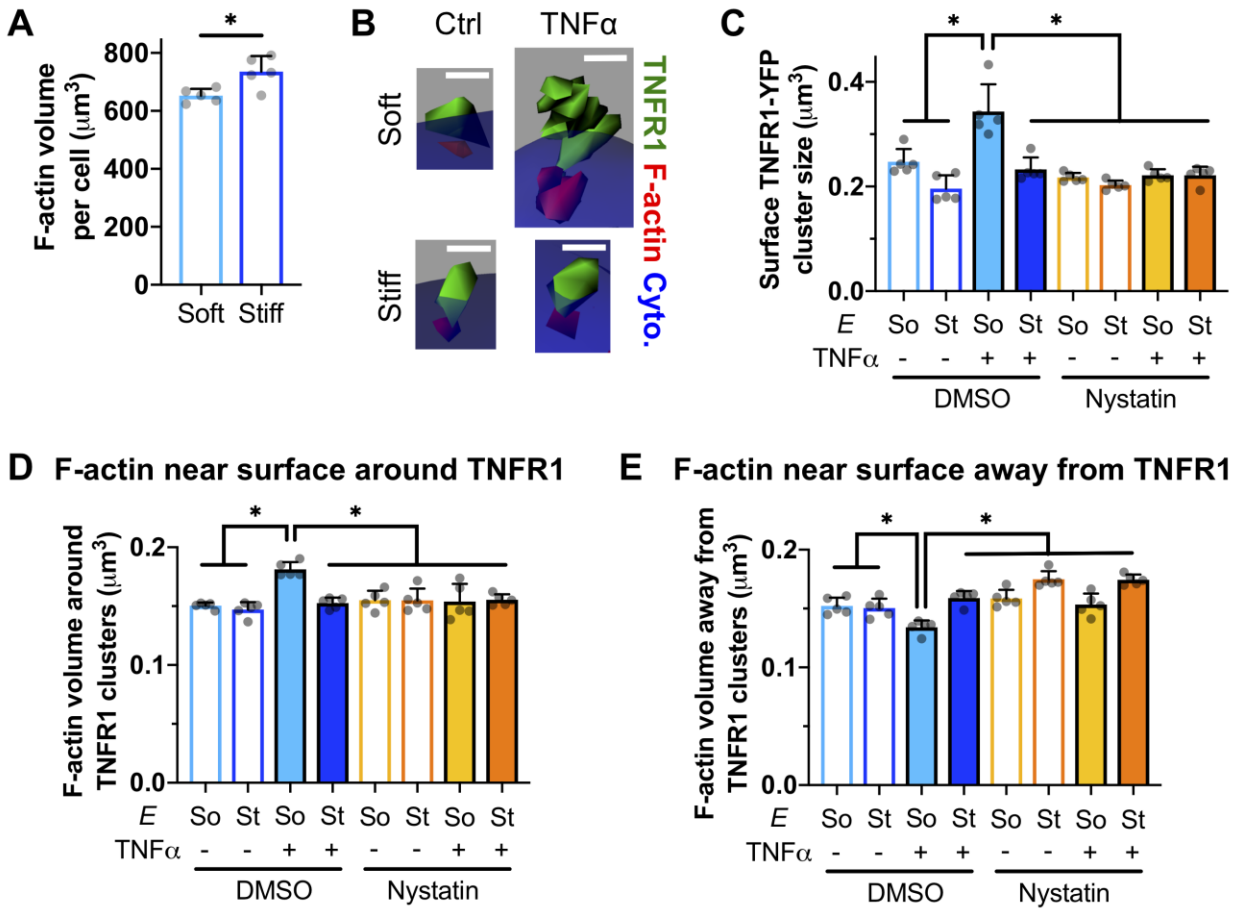

Figure S4. Characterization of TNFR1 and F-actin near the cell surface as a function of matrix stiffness and lipid rafts. (A) Total F-actin volume per cell in soft *vs*. stiff matrix measured by quantifying LifeAct-RFP signals from 3D reconstructed confocal images. Unpaired T-test, *P<0.05 soft *vs*. stiff (n = 5 cells from 2 experiments). Error bars: ± SD. **(B)** Representative confocal images from 3D construction showing TNFR1-YFP (green) on the outer boundary of the cytoplasm (CellTrace, blue), along with F-actin (LifeAct-RFP, red) adjacent to TNFR1-YFP. Scale bar = 0.5 μm. **(C)** Cluster size of TNFR1-YFP on the cell surface as a function of matrix stiffness, TNFα, and nystatin. Labeled MSCs in soft or stiff gels were preincubated with either DMSO or nystatin (50 μM) for 2 hours, followed by treatment with or without TNFα (100 ng/ml) for 20 min prior to confocal imaging (see **Methods**). **(D)** F-actin volume at the vicinity (within 2-μm^3) of TNFR1-YFP on the cell surface. (**E**) F-actin volume around the cell surface where TNFR1-YFP is not visible. For (C)-(E), P<0.05 from one-way ANOVA with Tukey's HSD test, *P<0.05 (n = 5 cells from 2 experiments, the mean value of each cell from at least 70 measurements). Error bars: ± SD.

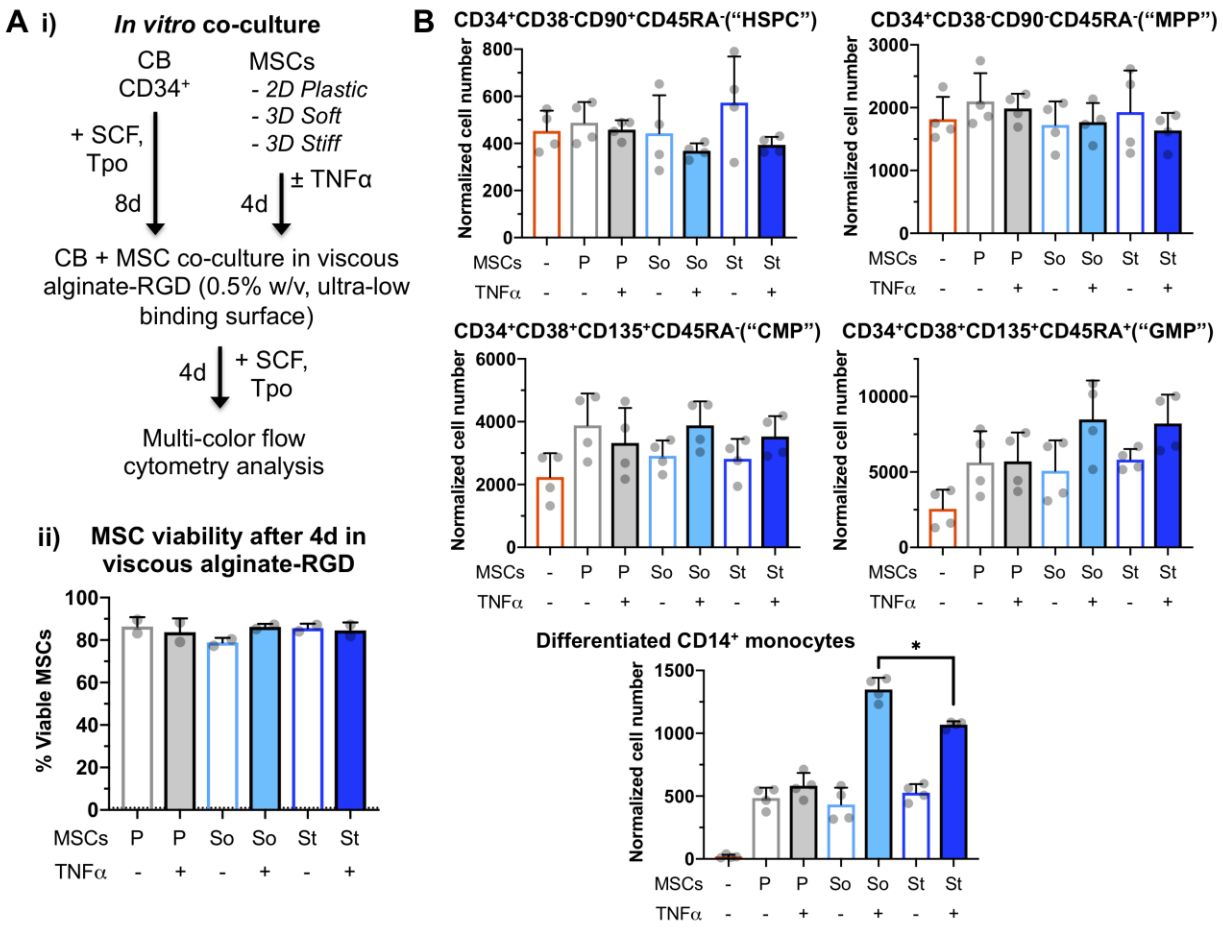

Figure S5. Effects of different culture environments on the ability of MSCs to impact hematopoiesis *in vitro*. (A) (i) Experimental Scheme (see **Methods**). CB: Cord Blood, SCF: Stem Cell Factor, Tpo: Thrombopoietin. (ii) Viability of primed MSCs after culturing in the alginate-RGD fluid (0.5% w/v) without gelation for 4 days. n = 2 technical replicates ± SD. **(B)** Quantification of different hematopoietic cell populations evaluated by multicolor flow cytometry. The indicated surface marker phenotypes are based on previous studies on human hematopoiesis (*33*, *34*). HSPC: Early hematopoietic stem progenitor cell, MPP: Multipotent progenitor, CMP: Common myeloid progenitor, GMP: granulocyte/monocyte progenitor. Cell number for each subpopulation was normalized to 5000 total CB cells precultured for 8 days prior to co-culture. For GMP and differentiated $CD14^+$ monocytes, $P<0.05$ from one-way Brown-Forsythe and Welch ANOVA with Dunnett T3 multiple comparisons test, $^*P<0.05$ (n = 4 pooled from 2 experiments). Error bars: ± SD.

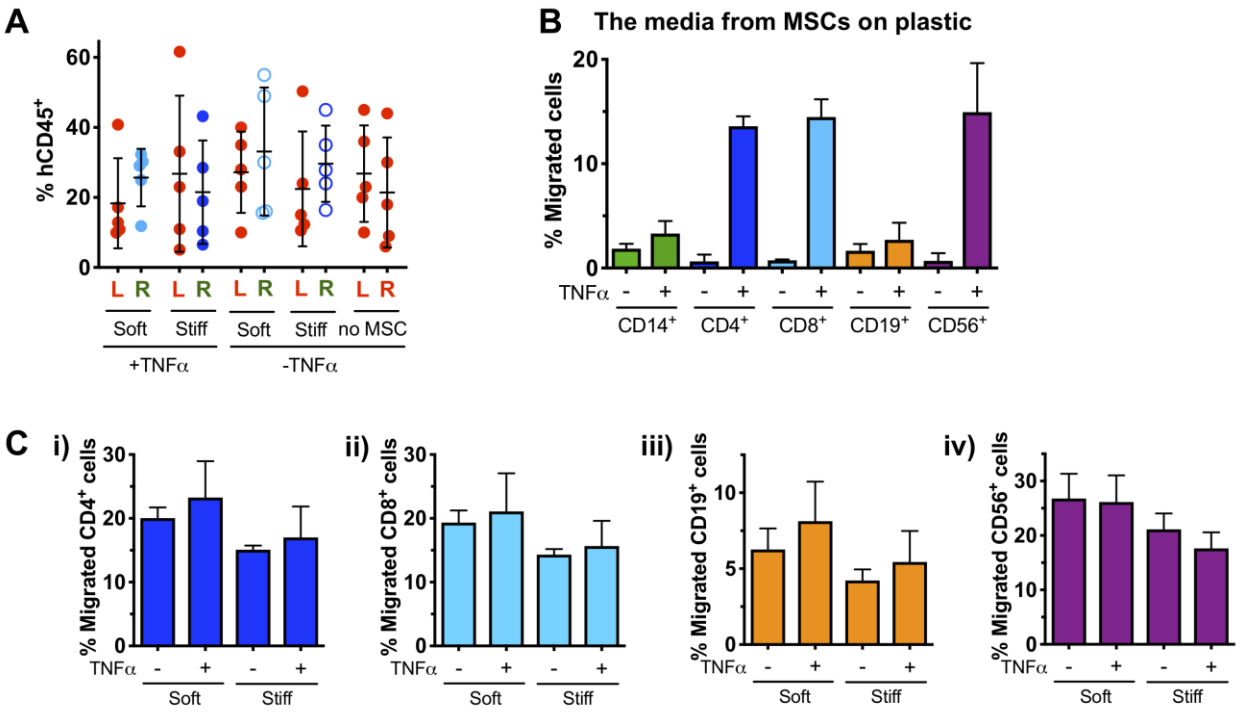

Figure S6. Characterization of human hematopoietic engraftment and chemotaxis. (A) Percentage of human $CD45^+$ ($hCD45^+$) cells in tibias relative to total $CD45^+$ cells (mouse $CD45^+$ cells and human $CD45^+$ cells). The analyses were done 4 days after PBS was delivered to the left tibia, and MSCs were delivered to the right tibia. n = 5 recipients from 2 independent experiments. **(B)** Percentage of migrated human peripheral mononuclear blood cell lineages towards the conditioned media from MSCs on plastic ± TNFα. n = 2 experiments ± SD. **(C)** The extent of lymphoid cell migration under chemotactic gradient through 3-μm pores for 3 hours. (i) $CD4^+$ cells. (ii) $CD8^+$ cells. (iii) $CD19^+$ cells. (iv) $CD56^+$ cells. n = 3 experiments ± SEM.

Table S1. List of primers for qPCR analysis

Gene (human)	Sequence (5' → 3')
CCL2	F: AAGATCTCAGTGCAGAGGCTCG R: TTGCTTGTCCAGGTGGTCCAT
CCL7	F: GAGAGCTACAGAAGGACCAC R: GTTTTCTTGTCCAGGTGCTTC
IL6	F: GGTACATCCTCGACGGCATCT R: GTGCCTCTTTGCTGCTTTCAC
IL8	F: ACTGAGAGTGATTGAGAGTGGAC R: AACCCTCTGCACCCAGTTTTC
TSG6	F: AATACAAGCTCACCTACGCAG R: GGTATCCAACTCTGCCCTTAG
TNFR1	F: TGCCAGGAGAAACAGAACAC R: TCCTCAGTGCCCTTAACATTC
CAV1	F: CCTTCCTCAGTTCCCTTAAAGC R: TGTAGATGTTGCCCTGTTCC
ANGPT1	F: AACCGAGCCTATTCACAGTATG R: ATCAGCACCGTGTAAGATCAG
CSF1	F: CGCTTCAGAGATAACACCCC R: TCATAGAAAGTTCGGACGCAG
CSF2	F: CTGAACCTGAGTAGAGACACTG R: GCCCTTGAGCTTGGTGAG
CSF3	F: TTCCTGCTCAAGTGCTTAGAG R: AGCTTGTAGGTGGCACAC
CXCL12	F: ACTCCAAACTGTGCCCTTC R: GACCCTCTCACATCTTGAACC
IL10	F: CGCATGTGAACTCCCTGG R: TAGATGCCTTTCTCTTGGAGC
IL11	F: CGGACAGGGAAGGGTTAAAG R: CACAGGCTCAGCACGAC
SCF	F: CCAGAACAGCTAAACGGAGTC R: GACGAGAGGATTAAATAGGAGCAG
VEGF	F: AGTCCAACATCACCATGCAG R: TTCCCTTTCCTCGAACTGATTT